Ore Geology Reviews 90 (2017) 287–306

Contents lists available at ScienceDirect

Ore Geology Reviews

journal homepage: www.elsevier.com/locate/oregeo

Genesis of Cr-bearing hydrogrossular-rich veins in a chromitite boulder from Ayios Stefanos, West Othris, Greece: A paradigm of micro-rodingites formation at the late stages of oceanic slab emplacement

Argyrios Kapsiotis [a,*], Anne Ewing Rassios [b], Giovanni Grieco [c], Aspasia Antonelou [d,e]

[a] School of Earth Science and Geological Engineering, Sun Yat-sen University, 510 275 Guangzhou, PR China
[b] Institute of Geology and Mineral Exploration, Lefkovrisi, 50100 Kozani, Greece
[c] Dipartimento di Scienze della Terra, Università degli Studi di Milano, via S. Botticelli, 23-20133 Milano, Italy
[d] Foundation for Research and Technology-Hellas, Institute of Chemical Engineering Sciences (FORTH/ICE-HT), P.O. Box 1414, GR-26504 Rio-Patras, Greece
[e] Department of Materials Science, University of Patras, GR-26504 Rio-Patras, Greece

ARTICLE INFO

Article history:
Received 2 May 2017
Received in revised form 25 May 2017
Accepted 6 June 2017
Available online 9 June 2017

Keywords:
Hydrogrossular
Cr-spinel
Rodingites
Chromitites
Ophiolites
Othris

ABSTRACT

The retired Ayios Stefanos chrome mine is hosted by deformed and serpentinized mantle peridotites of the western Othris ophiolite of central Greece. Chrome ores consist of m-scale lenticular to podiform chromitite bodies exposed within a tectonically attenuated dunite. We studied a mylonitized ore boulder (~2 m^3 in volume) that consists of massive-textured chromitite intruded by several altered gabbroic veins (≤15–20 cm thick). This chromitite boulder includes previously undescribed hydrogarnet-bearing microveins barely visible to the naked eye. The veinlets are isolated from each other and composed of undeformed Cr-rich hydrogrossular (spherules), clinochlore, serpentine, wollastonite, vesuvianite, brucite and subordinate amounts of other phases.

Textural observations of the intruding gabbros indicate that as tremolite substituted for diopside there was production of an oxidizing Ca-rich aqueous medium. This was capable of leaching Cr, Al and Fe^{2+} from Cr-spinel fragments dispersed within the veinlets. The resultant hydrothermal fluids transported components required to precipitate a mineral assemblage resembling that of rodingite. Hydrogrossular globules in the veinlets display chemical zoning characterized by increasing abundances of Cr_2O_3 and Fe_2O_3 and decreasing H_2O concentration toward their boundaries.

The en echelon structure of the micro-rodingite "arteries" combined with the unstrained nature of the veinlet minerals suggests that they filled late extensional cooling fractures in a mylonitized chromitite body. Overall, the structural-minerochemical characteristics of the veinlets can be adequately explained by general *T* decrease in the obducting slab concurrent to transport away from the spreading center.

1. Introduction

Aluminosilicate garnet-type compounds are important constituents of our planet's interior, from the crustal level to Transition Zone (TZ), and are considered as key mineral species in interpreting the genesis and petrological evolution of magmatic and metamorphic lithologies (e.g., Challis et al., 1995; Meyer and Boyd, 1972). The ophiolitic environment produces garnets of the ugrandite series that are commonly interpreted as a product of complex metasomatic reactions. These reactions are not well understood (e.g., Austrheim and Prestvik, 2008; Proenza et al., 1999), yet in the case of the Ayios Stefanos chrome ore bodies, they promise to aid in documentation of processes active within the late stages of lithospheric slab motions.

Ugrandite garnets are important mineral constituents of metasomatic lithologies known as rodingites. The consensus interpretation is that rodingites form when mafic rocks interact with rich-in-Ca and poor-in-SiO_2 hydrothermal fluids produced concurrent to serpentinization of associated ultramafic rocks (e.g., Coleman, 1967; O'Hanley et al., 1992). Some rodingites have been described that do not form by *in situ* replacement of pre-existing rocks (e.g., Bach and Klein, 2009; Pal and Das, 2010; Proenza et al., 1999). These conflicting origins provide insights into the driving forces of rodingitization processes (e.g., Frost and Beard, 2007).

Ugrandite-type garnet-dominant rodingite microveins were located within a massive chrome ore boulder of the Ayios Stefanos

* Corresponding author. Present address: Independent researcher, Ayiou Mina 31, 18900 Salamina, Greece.
E-mail addresses: kapsiotisa@yahoo.gr, kapsiotis@mail.sysu.edu.cn (A. Kapsiotis).

http://dx.doi.org/10.1016/j.oregeorev.2017.06.006
0169-1368/

mine in the Othris ophiolitic massif of central Greece, and found to incorporate significant amounts of Cr into their mineralogy. We note that Cr is not easily released from the Cr-spinel lattice and is customarily considered to be immobile in aqueous fluids (e.g., James, 2003). In the present work we document geological, compositional and Raman spectroscopy data of these microvein systems. Field relations between these microveins and their host rocks clarify the origin of the composite hydrogarnet-clinochlore-serpentine mineralization in the veinlet network. Compositional and spectroscopic information define the "physiognomy" of the process that stimulated Ca, Cr, Al, Ti and Fe^{2+} mobilization and enabled their re-concentration into a late veinlet system within chromitites that originated at mantle depths. Thus, the Ayios Stefanos deposits present an opportunity to better understand the activity and conditions of rodingitization taking place during a poorly known period in the evolution of the Othris lithospheric slab.

2. Geology of the Othris massif

2.1. General geology

The Othris Mountains are located in central Greece (Fig. 1); they are comprised of a nappe series representing the Pelagonian (Gondwana-derived) continental margin, offshore oceanic sedimentary series and Jurassic-aged remnants of a Tethyan ophiolite sequence (Rassios and Smith, 2000; Smith, 1979; Smith et al., 1975).

Nappes containing the Jurassic Othris ophiolite complex cover a total area of nearly 700 km^2 (Fig. 2). These nappes were emplaced in reverse lithostratigraphic order, that is, lower parts of the ophiolitic lithospheric section are emplaced over its higher members, as follows: (1) plagioclase lherzolites and lherzolites are found in the tectonically highest nappe sheet, and this sheet overlies; (2) a harzburgite nappe; (3) rocks of shallow lithospheric mantle origin; (4) ultramafic-mafic cumulates; (5) sheeted dikes, and (6) pillow lavas and flows often including Cu deposits typical of ridgecrest hydrothermal affinity. The ophiolitic nappe-unit rocks are emplaced over older lava and chert formations [the Agrilia formation of Smith (1979)] most likely associated with Permo-Triassic rifting and oceanic sedimentation along the margin of the Pelagonian continental mass (Fig. 2). Tectonically below the ophiolitic nappes at several localities is a mix of ophiolite-derived lithologies with oceanic sediments representing remnants of an accretionary mélange (i.e., Agoriani mélange; Ferrière et al., 1988). Amphibolite outcrops near Lamia and Metalleion have been interpreted as leftovers of the ophiolite's obduction sole. Dating of amphiboles from these sole rocks using the $^{40}Ar/^{39}Ar$ isotopic pair yielded ages of 169 ± 4 Ma (Spray et al., 1984). The entire nappe association was back thrust toward the SW over Eocene-aged flysch sediments (Rassios and Konstantopoulou, 1993; Fig. 2). In general, the Othris ophiolite has been regarded as a typical MORB-type oceanic lithosphere, though more recent studies document a more complex origin including SSZ-mantle domains (Barth et al., 2008).

The ophiolite sequence has no post-emplacement metamorphism. Ultramafic units are unaltered in some areas, and elsewhere

Fig. 1. Outline map showing the distribution of ophiolites in the southern part of the Balkan Peninsula (Vergely, 1976). Both Western Hellenic Ophiolites (WHO) and Eastern Hellenic Ophiolites (EHO) are shown with different colors. Key to lettering for Mesohellenic ophiolites: *V* Vourinos, *P* Pindos, *O* Othris.

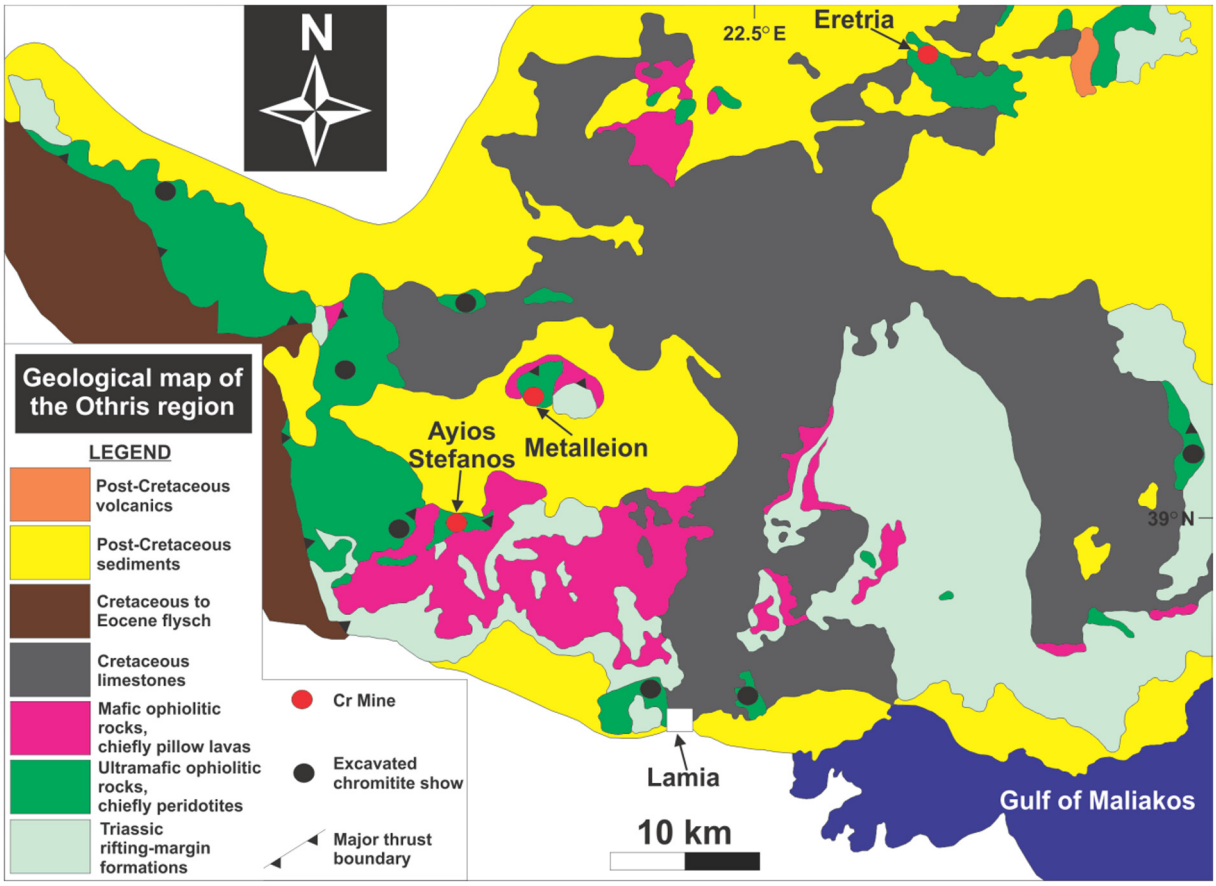

Fig. 2. Geological map of the Othris ophiolite complex (Rassios and Konstantopoulou, 1993).

considerably to totally serpentinized. Chromite deposits are rare; small shows of chrome ore have been located in dunites, but are nearly absent from large dunite bodies within harzburgite. Three (now abandoned) chrome mines within Othris produced ~1.5 Mt of ore (Fig. 2).

The preservation of deformation features dating to the ophiolitic slab movement (both ridgecrest and ductile to brittle off-ridgecrest) is particularly well defined within the nappe sheets. Deformational studies can be used to document lithospheric slab *P-T* conditions from the ridgecrest environment to the ductile/brittle limit (Rassios and Smith, 2000). The *P-T* conditions of brittle structures are less easily documented. Thus, a more comprehensive understanding of late-stage processes within the lithospheric slab is essential to the further modeling of the drift stage of ocean spreading and early obduction.

The formation of the Othris ophiolite and evolution of its nappe system remain enigmatic. Our present study of micro-rodingite veins, though they appear to be a minor detail, will significantly aid in the resolution of this puzzling evolution.

2.2. Geological outline of the Ayios Stefanos mine area

About 5×10^4 tons of Al-rich (refractory grade) chrome ore was exploited from the Ayios Stefanos mine in the 1950's up to the early 1960's. Chromite within the ore contains ~44–54 wt% Cr_2O_3 and ~16–24 wt% Al_2O_3. Ores assayed at 29–32 wt% Cr_2O_3 (Rassios, 2013). Today, ores are exhausted and the mine abandoned.

Ores are contained within ultramafic units associated with the mantle section of the Othris complex. The Ayios Stefanos mantle rocks cover a total area of approximately 2.5 km^2 (Fig. 3). The ultramafic unit consists of two peridotite thrust sheets: (i) the uppermost nappe is composed of plagioclase-bearing lherzolite, spinel-bearing lherzolite and minor harzburgite followed by subordinate dunite, and (ii) the lower thrust sheet is composed of harzburgite. The ultramafic nappes are separated by a well-exposed ductile-brittle thrust zone (Rassios and Dilek, 2009; Rassios and Konstantopoulou, 1993; Fig. 3). The thrust zone consists of highly tectonically attenuated (mylonitic) dunite (now completely serpentinized) and boudinaged chromitite ore bodies (Fig. 3). Chromitites within this zone are extensively deformed in evolving ductile to brittle conditions (Rassios and Konstantopoulou, 1993). Chromitite ores themselves are mylonitic-cataclastic in fabric, consisting of crushed remnants of the original mantle-derived chromite deposits.

The lithologies of both peridotite nappes show dark grey to dim green colors in the field, and are characterized by coarse-grained, strained mineral foliation. Deformation phenomena delineate ductile deformation related to motions concurrent to the origin of the tectonic contact/ore zone between the nappes. Such phenomena include ductile bowing of high *T* orthopyroxene form lines within the peridotite nappes (Rassios and Dilek, 2009), lower ductile *T* mylonitization and tectonic thinning of dunite within the ore zone, and pervasive ductile/brittle deformation-induced schistosity parallel to the thrust zone (Fig. 3). Orthopyroxene lineations have subhorizontal to moderately steep south-plunging orientations. Mylonitic structures within the ore zone have NE-SW plunging foliation planes, pointing toward dip-slip displacements. Mylonite zones (semi-ductile deformation) in the ultramafics parallel lithological contacts.

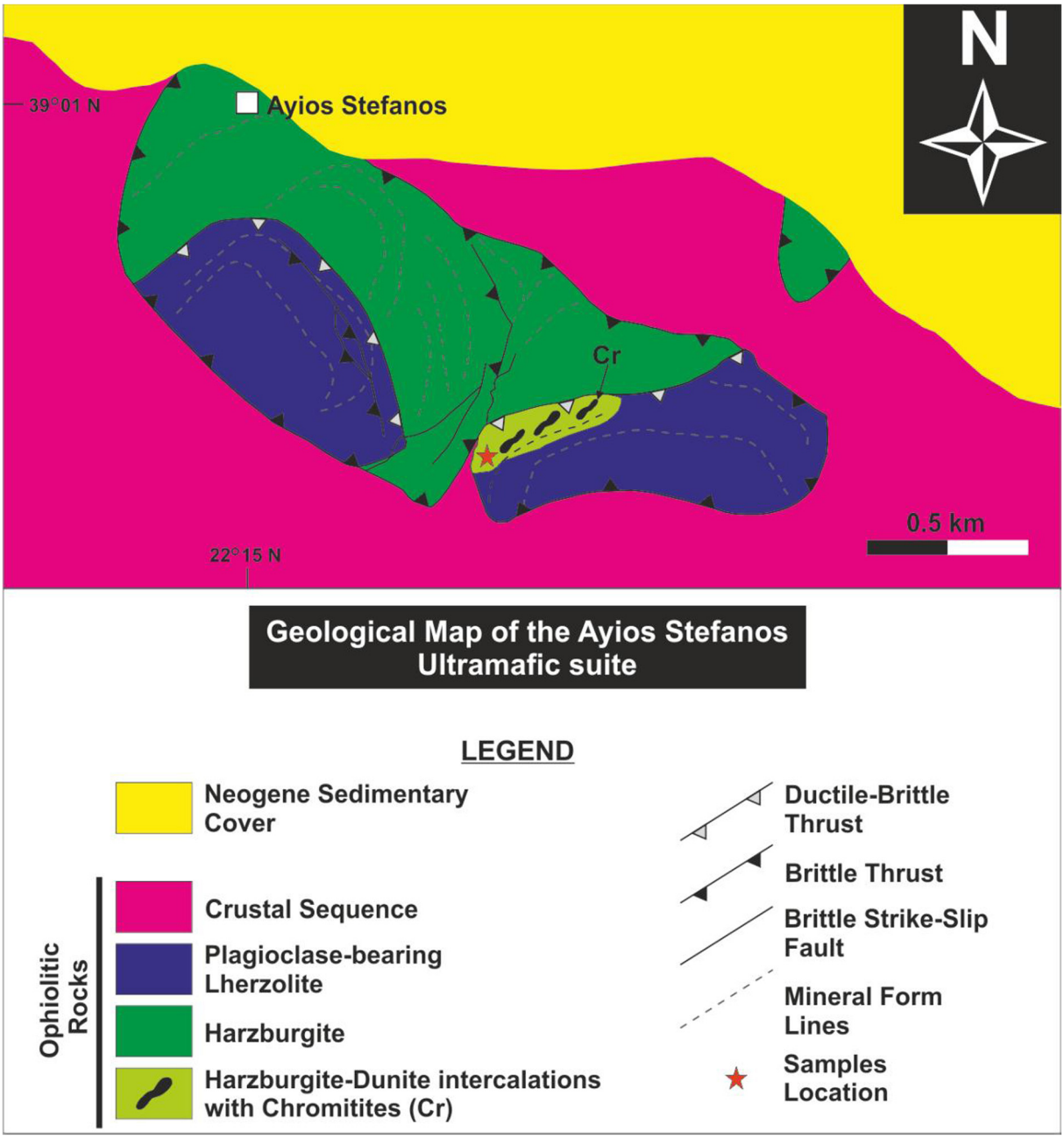

Fig. 3. Geological map of the Ayios Stefanos area demonstrating the bowing of structures synchronous to mantle nappe emplacement (Rassios and Dilek, 2009).

2.3. Field observations and sampling of chromitites and mafic rocks

Chromitites were collected from the open pit trench of the abandoned Ayios Stefanos chrome mine [latitude (φ): 39° 01′ 45″, longitude (λ): 22° 26′ 31″; Fig. 4a]. Several specimens were picked from remnant chromitite bodies within the tectonized dunite host. In addition, twelve ore samples were taken from a single chromitite boulder (Fig. 4b) preserved within the quarry talus.

The dunite host is around 30–50 m thick. Historic descriptions indicate that each chrome ore body within dunite was comprised of (semi-) massive chromitite of the scale of less than a m to several m, occurring as a series of elongated (sausage-shaped) discontinuous pods. At the southern end of the peridotite, well developed trails of ore bodies can still be tracked over a distance of a few hundred m, including some small-sized (less than 2 m thick) elongated pods (less than a few m long) concordant to the lineation fabric of the enclosing peridotites.

Mafic veins (≤15–20 cm-thick) are observed near and within the ore zone. These consist of white to pale-green coarse grained (crystal sizes ~1–2 cm) mafic plutonic material with sharp to diffuse outlines. The veins lack distinct modal or textural layering (Fig. 4b–c). On hand-specimen scale, Cr-spinel aggregates are discernible, apparently scavenged during intrusion through the host chromitites. The most impressive vein is one that intrudes a chromitite boulder (~2 m^3; Fig. 4b–c) within the quarry talus. It includes peridotite xenoliths (~10–20 cm-thick; Rassios and Dilek, 2009; Fig. 4b); the source of these mantle xenoliths could be their immediate host peridotite or some unreachable source in the upper mantle. Four specimens were collected from the mafic veins to examine their petrographic characteristics.

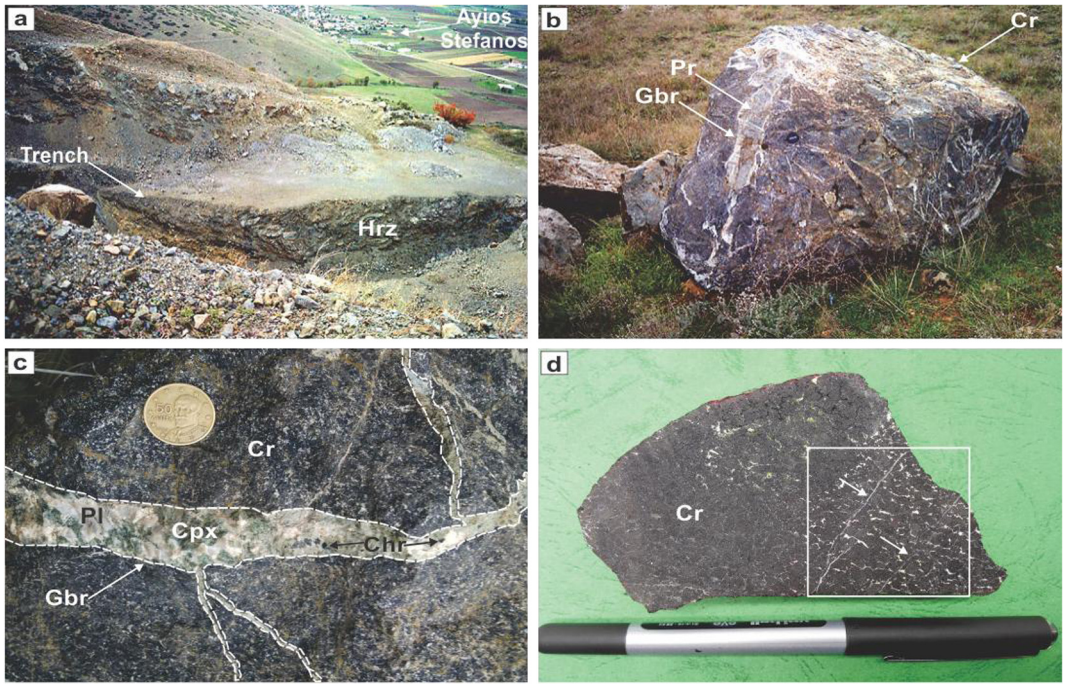

Fig. 4. (a) The Ayios Stefanos open pit chrome mine (the homonymous village can be seen in the background). (b) The studied chromitite boulder within the quarry talus. Note that the boulder is intruded by a network of coarse-grained gabbroic veins some of which host peridotite xenoliths. (c) Close up of a gabbro intrusion within the investigated chromitite boulder. Note the apparent lack of textural or mineralogical layering and the development of lateral ramifications branching off from the main gabbro intrusion. Chromian spinel aggregates scavenged by the chromitite host are also discernible. (d) Microveins (marked by the white, open square) cross cutting a chromitite specimen. Note that microveins are sub-parallel to each other. Abbreviations (henceforth in alphabetical order): *Cr* chromitite, *Chr* Cr-spinel aggregates, *Cpx* clinopyroxene, *Gbr* gabbro, *Hrz* harzburgite, *Pl* plagioclase, *Pr* peridotite.

2.4. Description of microveins

Microveins occur as a subtle but pervasive phenomenon in many of the chromitite ores. Actually, nine out of twelve samples collected from the chromitite boulder contained microveins that could be studied in detail (Table 1).

Microveins are barely observable to the naked eye. They cross cut all other textural features. Veinlets occur in sub-parallel sets with a spacing of several cm to dm, apertures of about 0.1–0.3 mm and lengths of a few tens of cm. When observable in hand-specimen, the veinlets appear white (Fig. 4d) to light green in color. Each appears independent; no microveins were observed to connect one to another (Fig. 4d). These microveins are exclusively located within chromitites cross cut by (altered) mafic intrusions suggesting the possibility that a genetic relationship exists between them and mafic veins. However, the mesoscopic features of the veinlets cannot be ascribed to (mafic) melt intrusion. For instance, their tips are nowhere directly associated with mafic veins, veinlets do not intrude the mafic veins, nor do the mafic intrusions cross cut microveins. Nevertheless, these veinlets

Table 1
Summary of the main petrographic characteristics of the investigated microveins. Abbreviations: *Brc* brucite, *Cal* calcite, *Chl* chlorite, *Grt* garnet, *Mlr* Millerite, *Ser* serpentine, *Syl* sylvite, *Ves* vesuvianite; *Wo* wollastonite. The following symbols: +++, ++ and +, stand for predominant, abundant and complementary mineral phase, respectively. The characters: o and –, denote the accessory presence and absence of a mineral phase, correspondingly. Superscript ([1]) is used to further clarify the meaning of the term "Grt-type compounds" that actually refers to various hydrougrandite species. Superscript ([2]) is used to delineate that non-finding of brucite cannot exclude its existence since brucite can actually be cryptically present (interlayered with serpentine).

Number of sample	Micro-structural description of veinlets	Predominant textures in veinlets	Grt-type compounds ([1])	Chl	Srp	Wo	Ves	Cal	Mlr	Brc ([2])	Syl	Petrographic observations (identification of the most typical microscopic characteristic)
1a	Asymmetric antitaxial	Interlocking (Srp)	+	++	+++	–	–	–	o	–	o	Resorption texture and porosity in Grt
2a	Symmetric antitaxial	Interlocking-bastite (Srp)/ Botryoidal-Spherulitic (Grt)	++	++	+++	++	–	–	–	o	–	Botryoidal aggregates of zoned Grt grains
2b	Composite	Fibrous-bastite	–	++	++	o	–	–	o	–	o	–
3a	Symmetric antitaxial	Botryoidal-Spherulitic (Grt)	+++	++	+	–	o	+	o	o	–	Multiple Chr fragments dispersed within the veinlets
3b	Symmetric antitaxial	Botryoidal-Spherulitic (Grt)	+++	++	+	–	–	+	o	–	–	–
3c	Asymmetric antitaxial	Banded (Grt-Chl)	+++	+++	+	–	–	o	o	–	–	Intercalations between Chl- and Grt-dominant layers
3d	Symmetric antitaxial	Botryoidal-Spherulitic (Grt)	+++	++	++	–	–	o	o	–	–	Local development of Grt-Cal intergrowths
4a	Composite	Fibrous (Srp)/Equigranular (Grt)	–	+	+	+++	–	–	–	o	–	Groundmass composed of Wo and Chl
6	Composite	Fibrous to stringy	–	++	++	o	o	–	–	–	–	–

attracted our attention because their morphological features and mineralization may be directly linked to processes that are active during some late stages in the life-cycle of an oceanic lithospheric slab.

3. Optical methods and analytical approach

Polished thin sections of all veinlet-hosting chromitite samples were studied by means of transmitted and reflected light optical microscopy and imaged using an OLYMPUS BX51 polarizing microscope. Back scattered electron (BSE) imaging of the specimens and line-scanning of various elements were done using a CARL ZEISS SIGMA scanning electron microscope (SEM) at the School of Earth Science and Geological Engineering, Sun Yat-sen University (SYSU), Guangzhou, P.R. of China. It was operating in the energy-dispersive spectroscopy (EDS) mode with an accelerating voltage of 15 kV and a bean current of 20 nA.

Quantitative mineral analyses were performed using a three-detector JEOL JXA-8800R electron probe micro-analyzer (EPMA) operating in the wavelength-dispersive spectroscopy (WDS) mode at the Instrumental Analysis and Research Center (IA & RC), SYSU. Operating conditions were 15 kV accelerating voltage and 20 nA beam current, with a beam diameter of 1 μm. The peak and background counting times were 10 and 5 s, respectively. Analysis of the investigated mineral phases for Al, Ca, Cr, Fe, K, Mg, Mn, Na, Ni, Si, Ti, V and Zn was done using the Kα X-ray lines of these elements. Natural albite, diopside, garnet, Cr-spinel, rhodonite, ilmenite and metallic V, Ni and Zn were used as reference materials. The standards were analyzed at regular intervals to check the precision of the acquired results. The following diffracting crystals were used: TAP for Al, Mg, Na and Si, PETJ for Ca, K and Ti, and LIFH for Cr, Fe, Mn, Ni, V and Zn. The detection limits are listed in the following as parts-per-million [(ppm): mg/kg, 10^{-6}]: Al = *ca.* 108, Ca = *ca.* 174, Cr = *ca.* 238, Fe = *ca.* 267, K = *ca.* 127, Mg = *ca.* 100, Mn = *ca.* 193, Na = *ca.* 142, Ni = *ca.* 229, Si = *ca.* 118, Ti = *ca.* 270, V = *ca.* 199 and Zn = *ca.* 486. These (are approximate detection limits that) were automatically calculated by JEOL software. The amounts of Fe^{3+} and Fe^{2+} in Cr-spinel were calculated assuming ideal spinel stoichiometry [$A^{2+}B_2^{3+}O_4$]. Analyses of Cr-spinel fragments from the microveins have been presented in a previous study about the genesis and post-magmatic alteration of the Ayios Stefanos chromitites (Kapsiotis et al., 2016). Recalculations for analyses corresponding to garnet-species were done using the GTcalc_corr.xlsx software of Locock (2008), a spreadsheet calculator that assigns molar percentages from chemical analyses based on the consideration of 29 garnet end-members. Data were corrected with a ZAF [atomic number (Z); absorption (A); fluorescence (F)] correction calculation. Analyses of garnet-type compounds, vesuvianite, wollastonite, chlorite and Cr-spinel from the investigated veinlets are provided in Tables 2–6 as supplementary files.

Raman analyses were done using a Renishaw inVia Raman Microscope at the Confocal Laser Raman Spectrometry Lab, (IA & RC) SYSU. Excitation was achieved using the 514 nm line of an Ar laser through a LEICA DMLM ×50 objective. The laser power was 5 mW and the collecting time 20 s. The scattered Raman light was collected in 180° back-scattering geometry and dispersed by a grating of 1800 grooves/mm. Spectra were acquired in the 50–1800, 50–4000 and 2800–4000 cm^{-1} regions with a spectral resolution of 2 cm^{-1}. The Raman OH^- vibration spectra were fitted with Gaussians until we achieved a random distribution of fitted residuals. Multiple spot analyses on different grains belonging to the same mineral species provided comparable spectra, thus indicating spectral reproducibility. Analyses were performed as many μm as possible away from the EMPA spots to avoid biased results due to possible structural changes caused by the electron beam.

4. Results

4.1. Petrography

4.1.1. Chromitite boulder

Chromitite within the ore boulder consists of 80–95 modal% of Cr-spinel. Chromian spinel grains are not larger than 6 mm in diameter; smaller grains occur within the margins of the ore boulder giving rise to a sintering texture. Under the microscope Cr-spinel grains have polygonal to rectangular crystal habits. Lobate boundaries on some Cr-spinel grains may imply subsolidus growth in the presence of fluids. Intense fragmentation of Cr-spinel is seen as brittle compressive cracks (Fig. 5a) that cross cut and offset large crystals. Along some of these cracks, recrystallization (Fig. 5b) and possibly grain recovery have occurred; this indicates mylonitic processes at relatively high *T* conditions.

The interstitial silicate groundmass of the chromitite is pervasively altered and no relicts of primary minerals have been preserved. This silicate mesostasis is mainly composed of serpentine and chlorite (Fig. 5c) with accessory tremolite, garnet, wollastonite and magnetite. The serpentine retains a pseudomorphic mesh texture after olivine (that is, with olivine boundaries currently delineated by magnetite-rich rims) and some bastite orthopyroxenes (Fig. 5d). Preservation of primary mineral characteristics in the silicate matrix of the investigated chromitites include: (i) retention of morphological outlines (mesh cells with a massive to granular shape) and crystal habits (prismatic bastite grains), (ii) retention of crystal sizes (bastite: ≤3 mm, mesh cells: ≤0.3 mm), (iii) preservation of strain characteristics such as undulose extinction and deformational twinning (in bastite), indicating mantle deformation processes, and (iv) the presence of bended clinopyroxene (exsolution) lamellae within bastite orthopyroxene. All these textural features are in agreement with typical olivine and orthopyroxene precursors for mesh and bastite serpentine, respectively.

Chlorite-tremolite intergrowths are commonly found dispersed within the silicate matrix. Tremolite substitutes partly for clinopyroxene lamellae exsolved from some former (now bastite) orthopyroxene crystals (Fig. 5e). Magnetite occurs in the form of trails among Cr-spinel grains. In cataclastic zones strongly fragmented Cr-spinels are locally cemented by garnet (Fig. 5f) or mixtures of garnet with chlorite, wollastonite and serpentine.

Chromian spinel in the examined chromitite specimens is seemingly unaffected by post-magmatic alteration processes. However, in one sample (out of 9 totally investigated) a few Cr-spinel grains show limited alteration to ferrian chromite (e.g., Mukherjee et al., 2010; Fig. 5e).

Most of the primary silicate inclusions in Cr-spinel grains [olivine, pyroxenes (enstatite, diopside), amphibole (edenitic pargasite), Na-bearing phlogopite (aspidolite)] have been altered to secondary mineral phases (chlorite and serpentine). One specimen was found to contain topotaxially aligned lamellae of rutile in Cr-spinel. These appear as fine-grained (≤0.4 μm thick, ≤25 μm long) needles developed in three crystallographic orientations, indicating that they represent exsolved minerals rather than inclusions within Cr-spinel (Kapsiotis et al., 2016).

4.1.2. Mafic veins

Plutonic mafic intrusions within the chrome ore boulder contain plagioclase and (altered) pyroxene. Modal analyses average at about 50–55% plagioclase, 35–40% clinopyroxene, less than 10% orthopyroxene, up to 5% Cr-spinel and trivial amounts of accessory Ti-rich minerals (predominantly titanite). These gabbro intrusions exhibit a coarse granular igneous fabric with random orientation of major mineral phases. Pyroxenes form subhedral to euhedral crystals (up to 1.3 cm) showing undulatory extinction

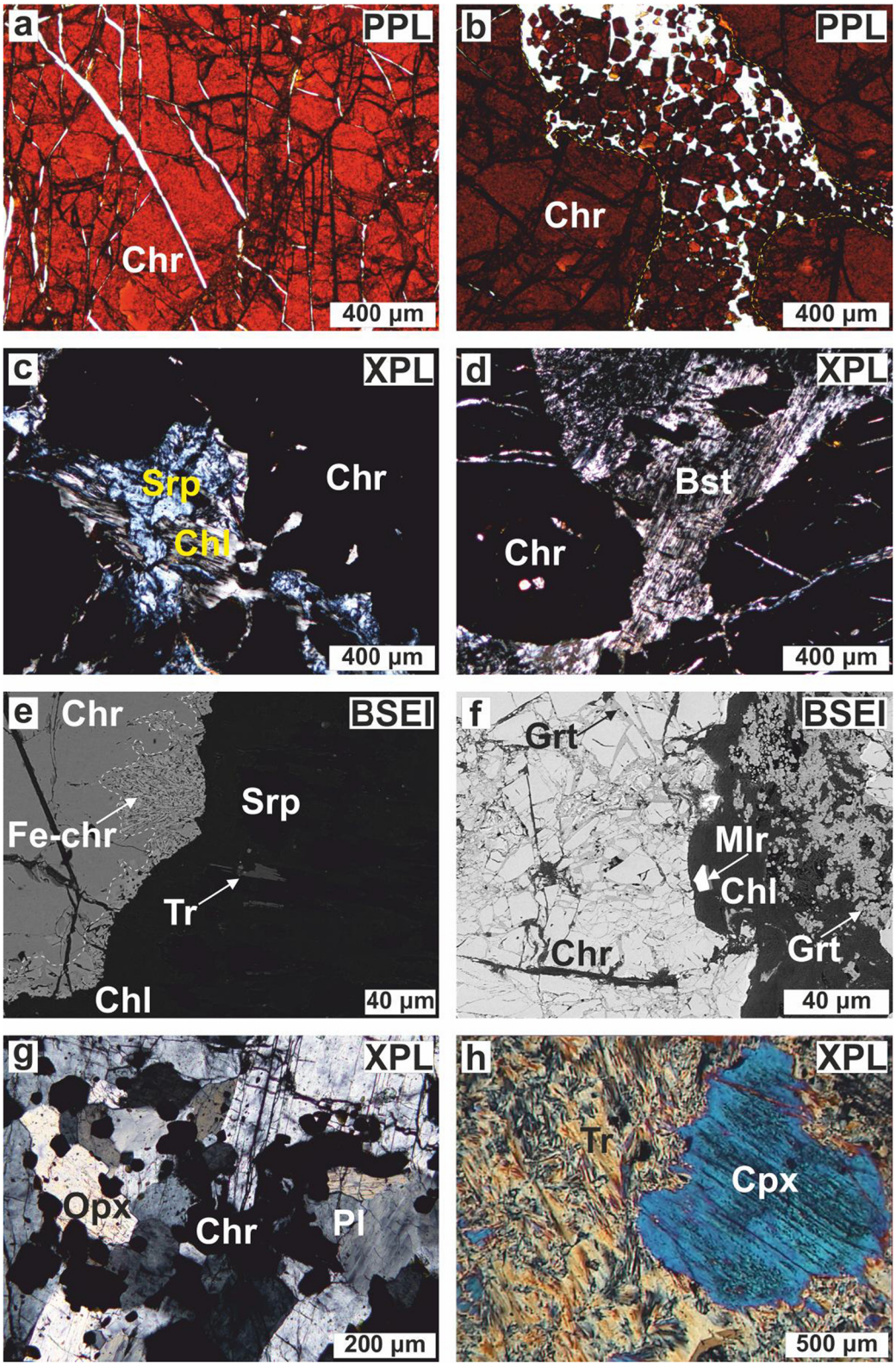

Fig. 5. Photomicrographs of the investigated chromitite boulder from the Ayios Stefanos ultramafic suite. (a) Strongly fractured Cr-spinel crystals. (b) Recrystallization phenomena on the boundaries of Cr-spinel grains (marked by the yellow dashed lines). (c) Serpentine cross cutting chlorite (clinochlore) in the altered silicate groundmass of the chromitite boulder. (d) Pseudomorphic substitution of serpentine for orthopyroxene leading to the development of bastite texture. (e) Chromian spinel grain showing limited alteration to ferrian chromite (marked by the white dashed line) across the boundaries. Note that some tremolite needles partly replace former clinopyroxene (exsolution) lamellae in bastite orthopyroxene. (f) Cementation of Cr-spinels in cataclastic zones by garnet. Note the alternation of a chlorite- with a garnet-dominant band in the nearby microvein. (g) Plagioclase along with a Cr-spinel aggregation derived from the chromitite host. (h) Imperfect replacement of clinopyroxene (close to extinction position) by tremolite. Abbreviations [following the system of abbreviations suggested by Whitney and Evans (2010)]: *Bst* bastite, *BSEI* back-scattered electron image, Chl chlorite, *Chr* Cr-spinel, *Cpx* clinopyroxene, *Fe-chr* ferrian chromite, *Grt* garnet, *Mlr* millerite, *Pl* plagioclase, *PPL* plane-polarized (transmitted) light, *Srp* serpentine, *Tr* tremolite, *XPL* cross-polarized (transmitted) light.

and twinning. Plagioclase occurs with a bimodal grain-size in which large (up to 1 cm) anhedral to subhedral grains are surrounded by much smaller (up to 0.3 mm) anidiomorphic grains. The latter occasionally display pressure (*P*) shadows (Fig. 5g). Chromian spinel is present as euhedral and spherical inclusions in pyroxenes or plagioclase and within aggregations of the host chromitite found along vein walls; these were apparently incorporated during intrusion (Fig. 5g). In a few samples, small (up to 100 μm) sphenoid titanite grains occasionally occur dispersed between plagioclase and clinopyroxene. Examination of these Ti-rich minerals under the SEM shows that they commonly exhibit limited porosity across their crystal boundaries.

The gabbro intrusions vary in degree and type of alteration; the type of alteration relates to the mineral undergoing modification. Primary clinopyroxene is nearly always completely replaced by alternating tremolite blades (Fig. 5h). Minor saussuritization has affected plagioclase. Plagioclase crystals are replaced by a complex and grayish to pasty green mineral mixture along brittle cracks. This mixture mainly consists of prehnite, zoisite, epidote and carbonates.

4.1.3. Microveins

Microveins demonstrate a fracture-filling, symmetric to asymmetric antitaxial structure within the chromitites (Table 1) and equigranular to fibrous internal texture. Their colors range from light yellow and purplish emerald to dark green (Fig. 6a). In microveins showing fibrous texture mineral grains present a well-developed preferred orientation. Mineral species observed during the microscopic study of the veinlets include (in decreasing abundance): garnet (-type compounds), chlorite and serpentine accompanied by wollastonite, vesuvianite and calcite, and accessory non-silicate phases including Cr-spinel, millerite (often desulfurized), hydroxides such as brucite and halides such as sylvite (Table 1).

Over the observable area of a single microvein, garnet appears to dominate. Several microveins demonstrate a banded structure consisting of a thin (<150–200 μm) chlorite-rich layer alternating with a relatively thicker, mainly garnet-dominant layer (Fig. 6b). The boundaries between these two layers are relatively sharp or even embayed. Occasionally voids may occur within the garnet-rich domains of the microveins, which are filled with chlorite or may represent former fluid inclusions. Overall, these mineralogical and petrographic characteristics (i.e., fibrous texture, banded structure) exclude a magmatic origin for the microveins. In contrast, they are supportive of a possible formation of the veinlets via precipitation of minerals by hydrothermal fluids at out of equilibrium conditions with the host chromitites (e.g., Python et al., 2007).

More specifically, garnets within the veinlets are bright green in color and commonly form subhedral to euhedral rhombic dodecahedra {110} with a maximum width up to 20 μm. These grains typically occur in the form of "cascades" of massive botryoidal aggregates that appear injected into the veins (Fig. 6c) and along some of their lateral fringes (Fig. 6d). Each botryoidal cluster is composed of garnet spherules aggregated against the veinlet walls or which appear to "float" within the main body of the microvein. Some clusters display quadrant anisotropic zones that have been described in the literature as characteristic of various types of natural hydrogarnets (e.g., Zabinski, 1966). Garnets within the aggregates display vitreous luster to the eye, extremely weak pleochroism and textural zoning under the microscope.

Zoning within garnet was discovered by observation of birefringence dissimilarities between cores and margins. While garnet cores are generally anisotropic, their rims are invariably opaque (possibly due to strain arising from lattice mismatch at compositional boundaries; Kitamura et al., 1986). In back scattered electron images (BSEI), zoned grains appear as tiny (<15 μm in size) globular particles that exhibit (mainly) two zones developed parallel to growing crystal faces (growth zoning; Fig. 6e). Individual garnet cores do not exceed 10 μm in diameter, whereas the surrounding concentrically developed rim(s) range(s) in thickness between 1 and 5 μm. In most cases, these demonstrate a rhombic dodecahedral inner dark core that has been overgrown by a higher-reflectivity outer zone with poorly defined outlines. The contact between core and rim is sharp and linear.

Garnets in the thickest parts of the veinlets exhibit resorption textures across their grain boundaries and are unevenly intersected by tiny serpentine (±chlorite) blades (Fig. 6f). In rare instances, the garnet spherules seem to have developed on tiny (<1–3 μm in size) Cr-spinel fragments or even (desulfurized) millerite particles. These appear to have served as "seeds" allowing garnet nucleation. In no case was garnet found to be statically forming at the expense of bastite orthopyroxene or any other mineral, and replacement textures are absent from the examined microveins.

Some garnet grains contain fluid inclusions less than 2 μm in size, most found in the core of the grains resembling those described by Melcher et al. (1997) in the chromitites of Kempirsai, Kazakhstan. Each inclusion is irregular in shape, and lacks connections to other inclusions. On inspection, some inclusions are fluid free, suggesting diffusion of their original fluid content after early trapping; such diffusion would be promoted in conditions of strain or heat (natural decrepitation). These observations are compatible with an origin of fluid entrapment during garnet precipitation (e.g., Zaeimnia et al., 2017). We emphasize that melt or composite fluid-melt inclusions were not found in garnets within the examined microveins.

Vein-filling chlorite occurs as purple- to brown-colored columnar crystals up to 150 μm in size that form intergrowths with garnet. Serpentine within the veinlets is yellowish to greyish, showing interlocking to stringy and fibrous texture, and is more common across the microvein margins often (cryptically) intergrown with brucite. Anhedral wollastonite with fuzzy boundaries has been found cementing garnet in the veinlets. Vesuvianite exhibits anomalous bluish-grey interference colors and forms mixtures with garnet. Garnet has been observed embedded in calcite in some veinlets (Fig. 6g). Chromian spinel fragments (80–500 μm in size) appear in the form of isolated crystals with smooth boundaries; however, the smaller of them appear as irregular-shaped grain wreckages, showing typical dissolution-replacement textures embedded in a matrix made of chlorite (Fig. 6h). In all cases the replacing phase was found to be a Cr-rich garnet-type compound (Fig. 6h).

Contacts between microveins and surrounding chromitite are generally smooth and planar, though sometimes may become somewhat curved.

4.2. Mineral chemistry

4.2.1. Hydrogarnet

Garnet-type minerals within the microveins display substantial intra- and intersample chemical inhomogeneity generally characterized by a pronounced deficiency in their analytical totals. This deficiency is ascribed to the presence of (an) undetected light element(s) or volatiles. Mineral compositions (Table 2 in the supplementary files) best correspond to garnet, but have calculated atomic formulae with a partial vacancy of the tetrahedrally coordinated position; theoretically, this site has to be completely filled with Si. The most common light element present in kenogarnet structure (Grew et al., 2013) is believed to be H^+ in the form of $(OH)_4$ groups that substitute for SiO_4 tetrahedra in the lattice of the mineral; possibly, this is the case for the vacant Si sites in the garnet within the examined veinlets. The low analytical totals

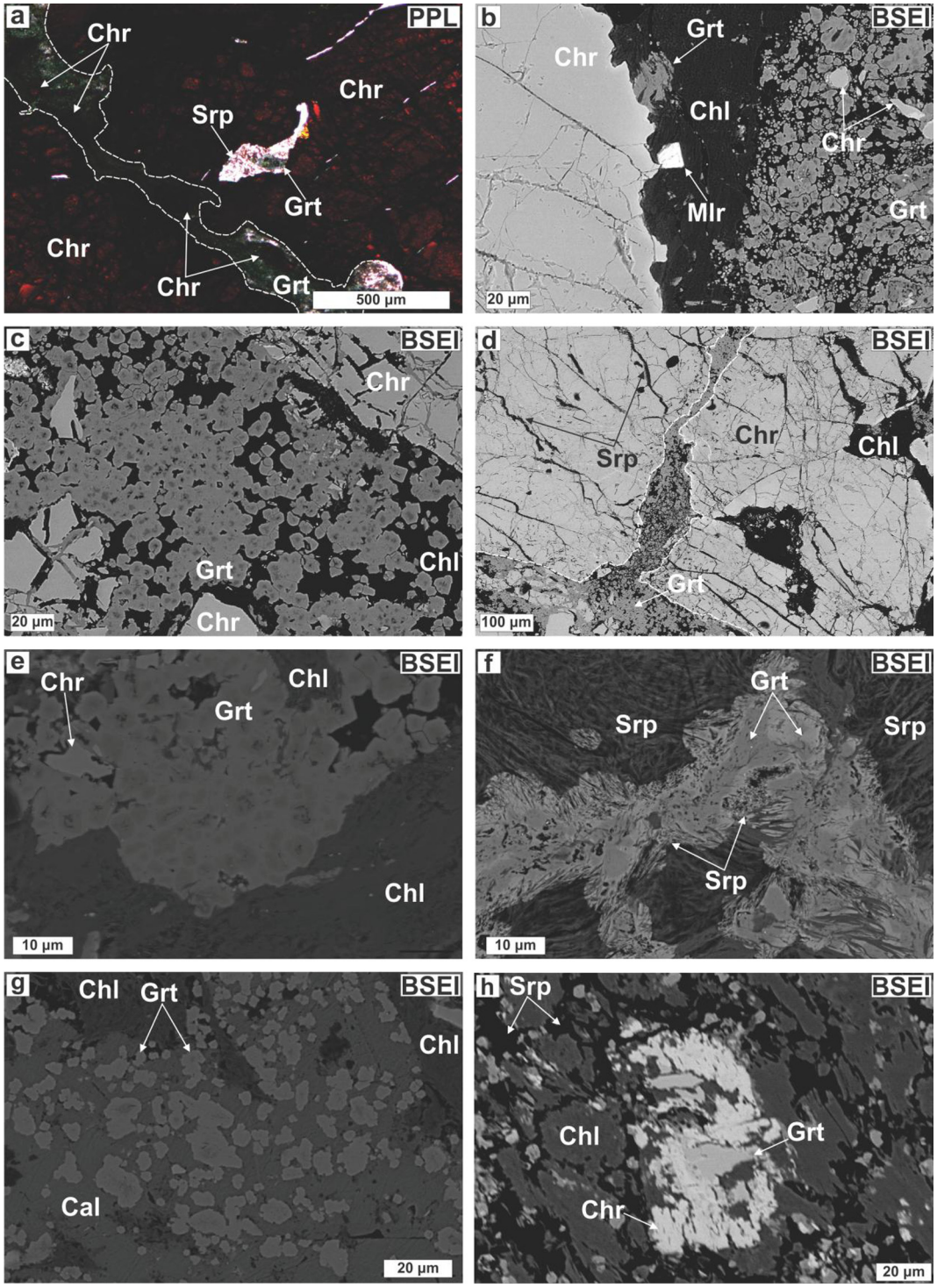

Fig. 6. Photomicrographs of the investigated hydrogrossular-rich veinlets. (a) Dark green veinlet with dispersed Cr-spinel fragments in its interior. (b) Banded microvein consisting of a thin chlorite-rich layer and a thicker, mainly garnet-dominant layer. (c) Botryoidal aggregates of garnet grains injected into the veinlets and (d) along some of their lateral fringes. (e) Garnet micro-spherules showing textural-compositional zoning. (f) Garnets within the veinlets exhibiting resorption texture across their grain boundaries unevenly intersected by serpentine fibres. (g) Garnet embedded in a matrix made up of calcite. (h) Irregular-shaped Cr-spinel relics replaced by Cr-rich garnet embedded in a matrix made up of chlorite. Abbreviations: *Cal* calcite (the rest as in previous figures).

combined with microscopic observations (i.e., anomalous birefringence, anisotropy) and spectroscopic data (see § "*4.3 Confocal Raman spectroscopy*") imply that these phases are hydrogarnets, the most common type of vacancy-dominant garnets. Their refractive index (Becke line of $n = 1.717$ on average) corresponds to hydrougrandite. Since thermogravimetric analyses (TGA) were not performed, the amount of H_2O was estimated as the difference from the ideal total of 100 wt%. Passaglia and Rinaldi (1984) concluded that the statistical deviation between the calculated abundance of H_2O in hydrogarnet by TGA analysis and difference from 100 wt% is minor (<1%).

The hydrogarnet grains show marked compositional differences, strongly dependent on their microtextural position. For example, the hydrogarnet spherules that fill the microveins are

characterized by a broad chemical range as follows: 33.07–40.19 wt% CaO, 28.33–35.90 wt% SiO_2, 7.77–16.83 wt% Al_2O_3, 5.49–13.41 wt% Cr_2O_3, 1.27–6.12 wt% Fe_2O_3; (original) totals vary between 91.39 and 97.82 wt% (Table 2 in the supplementary files). These hydrougrandites contain substantial amounts of H_2O implying that H^+ is mostly but not exclusively incorporated in their structure according to the coupled substitution: $4H^+ + {}^Z\square \rightarrow \square + {}^Z Si$ (known as hydrogarnet substitution; e.g., Lager et al., 1989). Our hydrogarnets have compositions intermediate between pure grossular and katoite [i.e., $(Ca_3)(Al_2)(Si_{3-x}\square_x)O_{12-4x}(OH)_{4x}$, where $1.5 < x < 3$] corresponding to Cr-rich hydrogrossular ($Adr_{0.00-17.85}Grs_{10.15-52.25}Kt_{9.43-34.92}Uv_{15.97-41.51}$). We will adopt the designation hydrogrossular for these microvein hydrogarnets following the logic of Dunn et al. (1985) that the term hydrogrossular would be acceptable for compositions along the grossular-katoite join.

Most of the hydrogrossular grains in the microveins demonstrate compositional zoning. This zoning is measurable as discrepancies in substances such as Al_2O_3, Cr_2O_3 and Fe_2O_3 from core to rim as follows: Al_2O_3 generally decreases from core to rim (7.77–16.83 wt% to 7.96–13.08 wt%), whereas Cr_2O_3 and (in most cases) Fe_2O_3 generally increase [5.49–12.54 wt% to 8.72–13.41 wt% and 1.27–5.90 wt% to 2.90–6.12 wt%, respectively (Table 2 in the supplementary files)]. Such variations indicate increase of both andradite and uvarovite molecules toward the grain peripheries. It is intriguing that except for the aforesaid oxides, analytical totals also

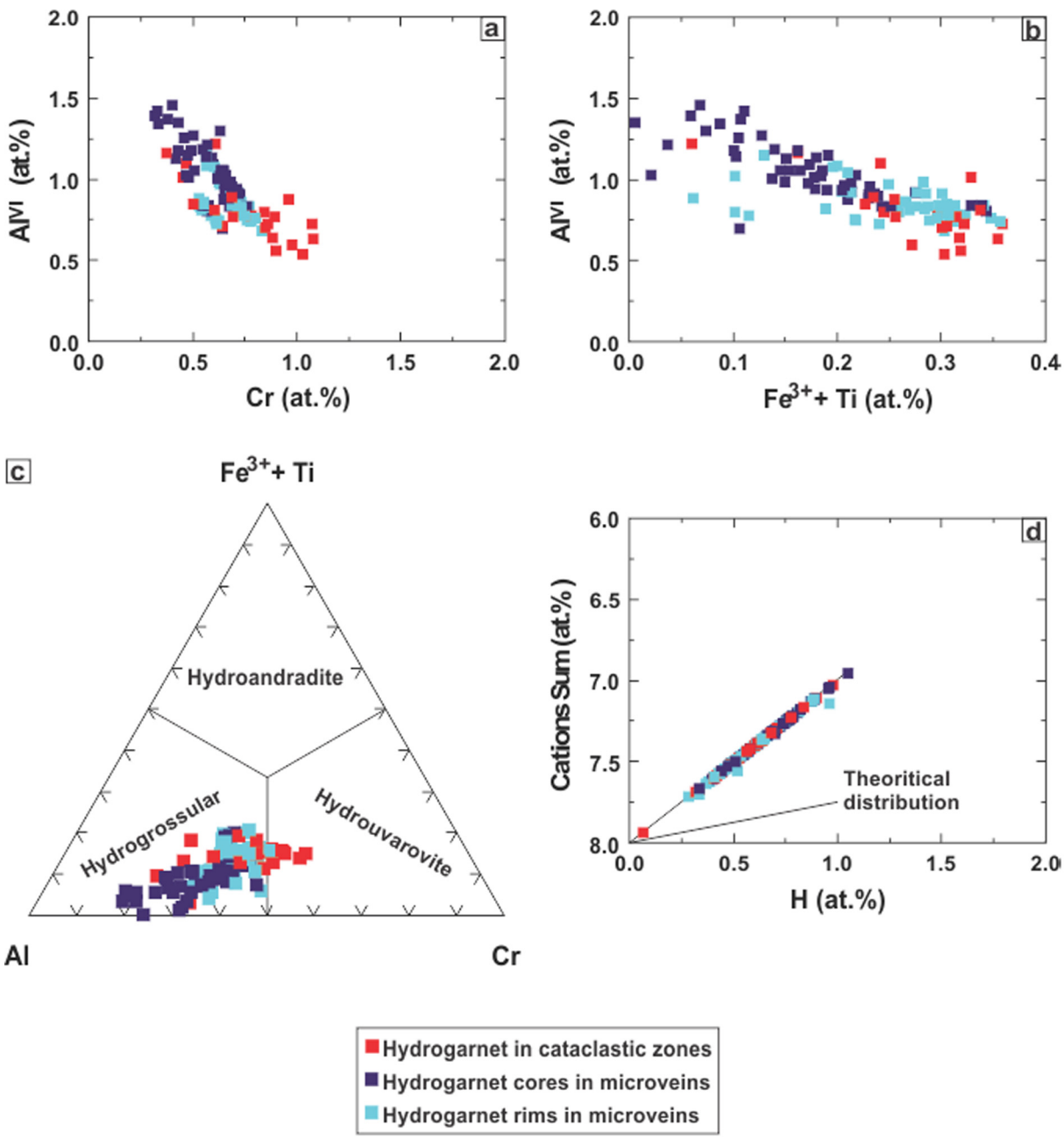

Fig. 7. Compositional characteristics of the analyzed hydrougrandites. (a) Covariation of Al^{VI} with Cr (at.%) at the Y (octahedral) site. (b) Covariation of Al^{VI} with (Fe^{3+} + Ti) at the Y (octahedral) site. In both diagrams a negative relationship is apparent, implying substitution of Cr and (Fe^{3+} + Ti) for Al^{VI}. (c) Classification of the analyzed hydrougrandites (mol.%) using the triangular diagram Al-Cr-(Fe^{3+} + Ti). (d) Cation sum *vs.* H (at.%) for the studied hydrougrandite compositions. Note the difference between the expected and acquired least-squares regression lines.

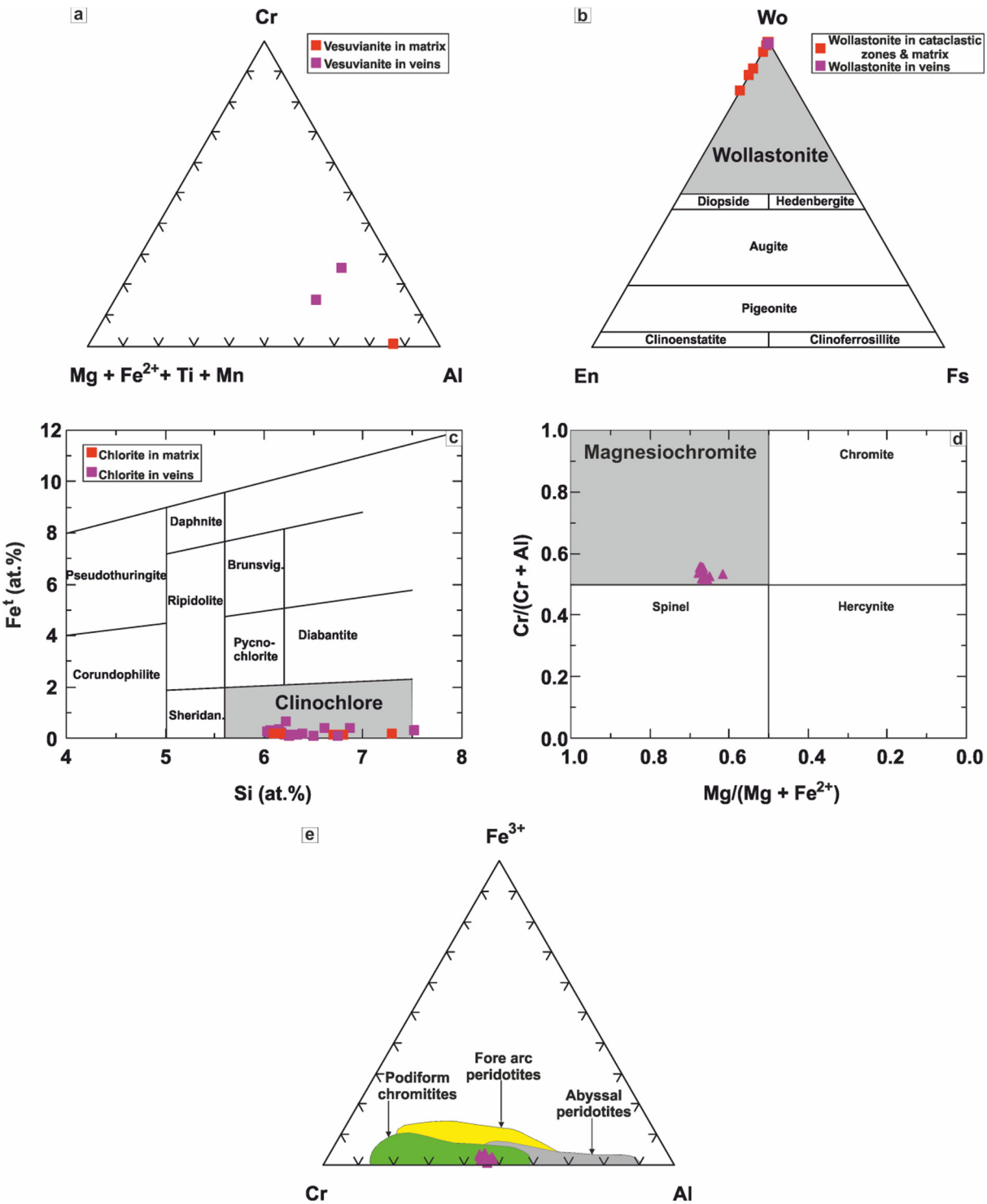

Fig. 8. Compositional characteristics of microvein-filling phases (except for hydrogarnet). (a) Plot of vesuvianite compositions on the Al-Cr-(Mg + Fe^{2+} + Ti + Mn) triangular diagram. (b) Plot of wollastonite compositions from cataclastic zones, matrix and veinlets on the Wo-En-Fs ternary diagram (Abbreviations: *Wo* wollastonite; *En* enstatite; *Fs* ferrosilite). (c) Chemical characterization of chlorite analyses from the chromitite matrix and microveins following the classification proposed by Bailey (1980). (d) Chemical variations and mineralogical classification of Cr-spinel fragments within veinlets in terms of Cr# [Cr/(Cr + Al) × 100] *vs.* Mg# [Mg/(Mg + Fe^{2+}) × 100]. (e) Plot of Cr-spinel fragments composition on the Al-Cr-Fe^{3+} triangular diagram. Fields of Cr-spinel composition from abyssal peridotites (Arai, 1994; Arai et al., 2011; Dick and Bullen, 1984), forearc peridotites (Arai et al., 2011) and podiform chromitites (Miura and Arai, 2014) are shown for comparison.

tend to increase from core to rim, thus implying that the spherules growth was essentially a dehydrating process. Theoretical predictions suggest that substitution of large cations (Cr^{3+}, Fe^{3+}, Ti^{4+}) for Al^{3+} in hydrogrossular (Fig. 7a–b) may lead to expansion of the crystal lattice, shifting the optimum stability toward anhydrous members (Heflik and Żabiński, 1969).

We have observed that hydrogarnet crystals in cataclastic zones also exhibit wide compositional variations as follows: 27.04–36.38 wt% SiO_2, 8.21–17.40 wt% Cr_2O_3, 4.62–7.23 wt% Fe_2O_3 and limited ranges in the subsequent major oxides: 33.62–38.70 wt% CaO and 7.51–10.84 wt% Al_2O_3, with (original) analytical totals that range from 93.41 to 97.56 wt% (Table 2 in the supplementary files).

These compositions generally correspond to Cr-rich hydrogrossular ($Adr_{3.67-16.88}Grs_{11.94-28.84}Kt_{10.58-27.97}Uv_{25.00-53.81}$), though some appear to correspond to an Al-rich variety of hydrouvarovite. We should note that water in natural uvarovite is limited (≤ 0.34 wt %; Andrut and Wildner, 2001), although the hydroxyl-dominant analogue of uvarovite has been experimentally synthesized (Morán-Miguélez et al., 1986).

Titanium-bearing hydrogrossular is another type of hydrogarnet found in cataclastic zones. The TiO_2 content in these hydrogarnets ranges from 0.89 to 3.22 wt%, indicating a high abundance of the morimotoite molecule(s) ($Adr_{0.38-7.38}Grs_{20.58-58.80}Kt_{2.20-32.59}$-$Mr_{0.00-5.70}Mg$-$Mr_{0.73-1.96}Uv_{18.80-30.43}$). Titanium-bearing hydrogrossular analyses show the following chemical variations: 27.45–37.95 wt% SiO_2, 36.34–39.36 wt% CaO, 11.52–13.33 wt% Al_2O_3, 6.37–9.90 wt% Cr_2O_3, 0.43–2.62 wt% Fe_2O_3, with (original) analytical totals varying between 92.11 and 99.49 wt% (Table 2 in the supplementary files).

Plots of these analyses onto the ternary system Al-Cr-(Fe^{3+} + Ti) demonstrate that compositions fall within the Cr-rich hydrogrossular and Al-rich hydrouvarovite fields (Fig. 7c). Hydrogarnet substitution alone cannot sufficiently explain incorporation of H^+ into the lattice of hydrougrandites. Additional mechanisms are necessary to explain the substantial deviation between the theoretically expected hydrogarnet chemistry (based on the formula $X_3Y_2Z_{3-n}H_{4n}O_{12}$) and the chemistry of the mineral in our samples (Fig. 7d). Possibly, the current data indicate the presence of OH^- in other positions except for the tetrahedral in hydrogarnet structure. However, even this interpretation is commonly linked to hydrogarnets containing low amounts of water.

4.2.2. Vesuvianite

The compositional variation of vesuvianite ranges as follows: 30.43–31.97 wt% SiO_2, 13.56–22.06 wt% Al_2O_3, 0.27–8.70 wt% Cr_2O_3, 1.01–5.31 wt% MgO and 0.19–3.06 wt% FeO^t (Table 3 in the supplementary files; Fig. 8a). Low analytical totals (91.53–94.48 wt%) are due to the presence of volatile components.

4.2.3. Wollastonite

Wollastonite composition differs between that in microveins and that in cataclastic zones (Fig. 8b). Wollastonite in the microveins shows a near constant, lower content of SiO_2 and CaO (SiO_2: 49.81–51.34 wt%, CaO: 46.49–48.74 wt%) compared to wollastonite cementing cataclastic zones (SiO_2: 50.83–53.93 wt%, CaO: 46.33–49.21 wt%). Wollastonite in the matrix has higher SiO_2 content (54.79–57.19 wt%) compared to the same mineral in microveins and cataclastic zones, but significantly lower CaO content (36.65–42.38 wt%; Table 4 in the supplementary files). Wollastonite analyses reveal minor bustamite [(CaMn)SiO_3] substitution (MnO: ≤0.03 wt%, FeO^t: ≤0.11 wt% and Al_2O_3: ≤0.54 wt%; Table 4 in the supplementary files).

4.2.4. Chlorite

Chlorite in microveins demonstrates a broad variation in SiO_2 (30.00–40.71 wt%), Al_2O_3 (8.59–21.63 wt%) and MgO (24.82–33.47 wt%; see Table 5 in the supplementary files). The Cr_2O_3 concentration reaches up to 12.76 wt%. Both FeO^t and NiO contents vary from 0.59–3.72 wt% and 0.05–0.50 wt%, correspondingly. The CaO content in the vein-filling chlorite is up to 2.21 wt%. Chlorite in the mylonitic matrix shows no chemical dissimilarities with

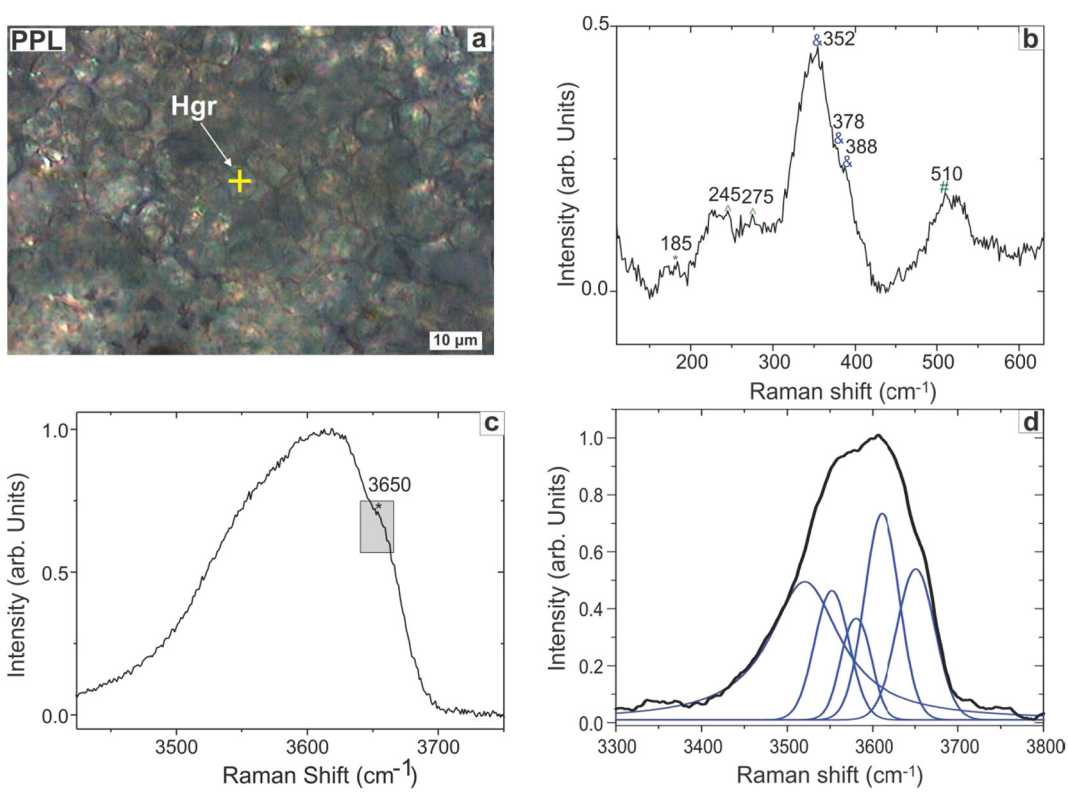

Fig. 9. (a) Transmitted light photomicrograph of a massive aggregate composed of emerald green hydrogrossular. Abbreviations: *Hgr* hydrogrossular (the rest as in previous figures). (b) Representative Raman spectra for the hydrogrossular grain marked by the yellow cross in the previous image in the region up to 650 cm^{-1}. (c) Representative Raman spectra of the same hydrogrossular grain in the interval between 3425 and 3750 cm^{-1}. (d) Deconvolution of the ~ 3600 cm^{-1} peak using the Gaussian mode. The appearance of several peaks implies OH^{-1} defects in crystal structure. Mind the presence of a noticeable band at ~3650 cm^{-1}, which corresponds to the presence of OH^-.

the vein-filling chlorite (Fig. 8c). The most striking chemical difference between chlorite in the microveins and that in the matrix is a lower Cr_2O_3 content in the former (1.63–2.63 wt%) compared to the latter (≤12.76 wt%; Table 5 in the supplementary files). Chlorite analyses straddle the boundaries between the compositional fields of sheridanite and clinochlore (Fig. 8c), their best grouping is as clinochlore following the classification of Bailey (1980).

4.2.5. Chromian spinel (Cr-spinel)

Analyses of Cr-spinel fragments dispersed within the microveins are homogenous (Cr_2O_3: 42.51–45.52 wt%, Al_2O_3: 23.84–26.82 wt%, MgO: 13.67–14.95 wt% and FeO^t: 14.13–15.72 wt%; Table 6 in the supplementary files). Chromian spinel has Cr# [Cr/(Cr + Al) × 100] values that range between 51.67 and 55.82, Mg# [Mg/(Mg + Fe^{2+}) × 100] values varying from 61.56 to 67.74 (Fig. 8d), and low Fe^{3+}# [Fe^{3+}/(Fe^{3+} + Cr + Al) × 100] values (≤19). These correspond to magnesiochromite with significant proportion of the spinel constituent (Fig. 8d). The composition of Cr-spinel fragments within the veinlets is analogous to that observed in mantle-hosted (podiform) chromitites from other ophiolites (Fig. 8e). Microvein Cr-spinel fragments are characterized by limited TiO_2 (≤0.12 wt%), which is another typical compositional feature of Cr-spinel from many ophiolitic chromitites (< 0.30 wt% TiO_2; Leblanc and Nicolas, 1992). They do not appear altered in petrographic examination and their relatively high Mg# suggests a lack in post-vein Cr-spinel alteration (e.g., Barnes, 2000). Regardless of their size or texture, the Cr-spinel fragments in microveins are similar in composition to the Cr-spinel comprising the host to the veinlets (Kapsiotis et al., 2016).

4.3. Confocal Raman spectroscopy

A number of Raman spectra were acquired from garnet-type minerals within the microveins (Fig. 9a). These display bands best attributed to intermediate species between the grossular and katoite end-members. A band at 185 cm^{-1} plausibly corresponds to T(SiO_4) in grossular, whereas bands at 245 and 275 cm^{-1} are best interpreted as Ca vibrations (Fig. 9b; Kolesov and Geiger, 2005). According to Kolesov and Geiger (1998), the wavenumbers of the Ca modes in hydrogrossular should not be considerably different from those in grossular and andradite, located between 240 and 320 cm^{-1}. Bands at 352 and 378 cm^{-1} should be assigned to the R(SiO_4) mode in grossular. A band peak at 388 cm^{-1} probably represents mixed T/R(O_4H_4) modes in katoite. The band between 510 and 530 cm^{-1} approximates the bending mode of SiO_4 polyhedra in grossular (Fig. 9b). Bands between 800 and 1100 cm^{-1} can also be ascribed to the Si-O stretching mode in grossular (Kolesov and Geiger, 1998; 2005).

Although the Raman modes for garnet-like minerals in the veinlets are best interpreted as representing grossular, deconvolution of the asymmetric bands at the high frequency region of the spectra implies the existence of water in accordance with our analytical data. Nearly all garnet spectra exhibit internal O–H stretching bands at approximately 3650 cm^{-1} that have shapes consistent with a combination of molecular water and OH^- groups vibrational modes (Fig. 9c). After deconvolution, several O–H bands appear that can be ascribed to various OH^- defects in the structure of hydrogrossular (Fig. 9d; e.g., Thomas et al., 2008). The main band of the O–H stretching (F_{2g}) mode at 3650 cm^{-1} reveals the presence of water in our garnet compounds.

Raman band positions for the analyzed hydrogarnets are expected to substantially deviate from those of pure grossular or unadulterated hydrous ugrandites, especially katoite. Minor substitution of Fe^{2+}, Mn and Mg for Ca can result in additional band position shifts setting the final spectra apart from those of both ideal grossular and katoite.

Raman spectroscopy is appropriate only for qualitative estimation of the H_2O content in hydrogarnets (Arredondo and Rossman, 2002); the weak intensity of O–H stretching bands in these hydrogarnets does not correlate to the compositional abundance of H_2O incorporated in their structure.

Lizardite is the dominant serpentine polymorph identified under Raman spectroscopy, exhibiting peaks at the high-frequency spectra domain (i.e., 3688 and 3705 cm^{-1}; not shown here). No characteristic peaks for CO_2 (at 1388 and 1285 cm^{-1}) or organic matter (i.e., 1392 and 1590 cm^{-1}) were detected.

5. Discussion

5.1. Intrusion of the Ayios Stefanos gabbroic vein network

The ductile–brittle thrust at Ayios Stefanos correlates in position to a (serpentinized) dunitic unit (Rassios and Dilek, 2009; Fig. 3) hosting chromitites. Dunite is less-competent than its footwall and hanging wall peridotites and appears to have been tectonically thinned. This process resulted in mylonitization of the chromitite bodies hosted in dunite.

The ductile–brittle thrust was intruded by a network of anastomosing gabbroic veins, which are more common in the harzburgite footwall than the plagioclase-bearing lherzolite thrust sheet. Some gabbroic veins penetrated the chromitite bodies (Fig. 4b–c). These veins do not display "topographic" intrusional boundaries or internal petrologic layering as for typical cumulate intrusions (Rassios, 1981). In fact, they have a complex morphology developing multiple lateral ramifications (Fig. 4c). These appear to represent minor volumes of melt, instantaneously squeezed out of the main gabbro intrusion by active tectonic forces causing the opening of fractures.

Field and macroscopic observations confirm that the gabbroic veins at Ayios Stefanos are deformed. This deformation is not as intensive as that of the other constituents of the ductile–brittle thrust, but is conformable with imprinting deformation at a late stage of movement between the nappes. We thus interpret these veins to be *syn*-kinematically emplaced into a moderately hot environment under semi-ductile to brittle conditions (e.g., Mondal et al., 2001; Mondal and Zhou, 2010).

5.2. Intrusion of the hydrogrossular-rich microveins

5.2.1. Implications from the veinlets micro-structural characteristics

Unlike the gabbro intrusions, microveins are filled with non-magmatic minerals (hydrogarnet, chlorite, serpentine and wollastonite), so their formation postdates that of the mafic intrusions. Further evidence for this comes from the absence of melt and/or melt-fluid inclusions from hydrogarnet within the investigated microveins, excluding a magmatic origin for the hydrogarnet spherules.

Crystal growth direction within the microveins in the chromitite boulder is symmetric to asymmetric antitaxial; veinlet mineral phases grew out (mainly) from the center toward the microvein walls. Nucleation associated with incremental opening of veins can produce banded structures as those present in some specimens (Fig. 6b). Growth competition in such tight environments is expected to result in a preferred orientation of grains perpendicular to the vein margins, as is also observed in some samples. These kinds of textures imply that the microveins resulted from a single, late fracturing episode that provided the necessary space for the veinlet fluids and for the minerals to grow. None of the microveins demonstrate deformation and the veinlet minerals themselves show undeformed (crystal growth) textures. The en echelon nature of the veinlets suggests that they filled extensional cooling fractures in the mylonitized chrome ore bodies.

Different scenarios could explain the transition from microvein domains made up mainly of clinochlore to domains composed predominantly of hydrogrossular aggregates. One scenario would involve the prevalence of strong concentration gradients within a single pulse of the vein-filling fluid (e.g., Plümper et al., 2014). An alternative hypothesis necessitates consecutive but non-periodic influxes of fluids, with the influx succession recurring several times across the length of a single veinlet. Possible support for this scenario arises from the documentation of the absence of hydrogrossular spherules from the tips of the studied "arteries".

5.2.2. Genesis of micro-rodingites

Calcium-rich aluminosilicates (hydrougrandites, vesuvianite), wollastonite, and low-silica phases (clinochlore, serpentine and brucite) were documented within the microveins (Table 1). The coexistence of these minerals in the microveins requires the existence of a focused influx characterized by substantial Ca-enrichment and concurrent Si-depletion. Mineral assemblages of this sort have been documented within metasomatic lithologies known as rodingites (e.g., Coleman, 1977; Li et al., 2007; O'Hanley et al., 1992). Indeed, the occurrence of hydrogrossular is virtually diagnostic for the definition of rodingite lithologies (Frost and Beard, 2007).

Rodingites commonly form in peridotites in association with the occurrence of gabbro or dolerite intrusions undergoing serpentinization; that is, the serpentinization process provides fluids that are also responsible for the metasomatism of intrusions within the peridotite body (e.g., Coleman, 1967). Rodingitization-related fluids that are moving upwards from a permeable serpentinization front will precipitate brucite because of their low silica activity (Frost and Beard, 2007); in cases where the *T* is low and the fluid is sufficiently rich in Ca, andradite will crystallize (Beard and Hopkinson, 2000). In the Ayios Stefanos microveins we have documented the coexistence of brucite and hydrougrandite spherules with relatively high abundance of Fe_2O_3 at their rims; this supports a rodingitization-related fluid produced almost concurrently to serpentinization.

Rodingitization is relatively widespread within the Othris ophiolitic serpentinites (e.g., Koutsovitis et al., 2013), though gabbro and dolerite intrusions are generally rare. At Ayios Stefanos, we have described the conditions in which gabbroic magma of mantle origin penetrated the chromitite host to the rodingite veinlets. Could the alteration of gabbro contributed to the genesis of the micro-rodingites? The lack of replacement textures in the microveins strengthens the interpretation that they originated when open cracks became filled with a circulating post-magmatic fluid causing crystallization of rodingites.

Petrographic observations document that rodingite formation within the microveins initiates with the crystallization of hydrogrossular and terminates with the precipitation of Mg-rich silicates. This sequence indicates a low silica activity system as the driving force of mineral paragenesis within the veinlets (e.g., Frost and Beard, 2007). The progressive depletion of Ca, Cr and Fe^{3+} coupled with a residual increase in the Mg content of the fluid propelled clinochlore precipitation in the veinlet boundaries. These boundaries are alike to the chlorite-rich zones observed on mesoscopic scale in rodingites from East Othris (Koutsovitis et al., 2013) and quite similar to the so-called "black-walls" (Frost, 1975) commonly developed along mafic-ultramafic contact zones undergoing serpentinization or fissures filled with serpentinization-derived fluids (e.g., Austrheim and Prestvik, 2008; Bach and Klein, 2009).

The extreme rarity of micro-rodingite veins in the Ayios Stefanos mantle suite implies that the parent fluid was low in volume and rapidly consumed. In fact, only small volumes of a hypothetical fluid source are needed to give rise to the formation of mineralized microveins. The presence of wollastonite and the limited occurrence of hydrogarnet in the cataclastic zones around microveins suggest a rapid decline in the Cr-Fe^{3+} potential of the fluid away from the veinlets. The conditions for micro-rodingites formation were very ephemeral pointing toward variable rates of nucleation and growth, diagnostic of non equilibrium conditions (i.e., crystallization of spherules; Python et al., 2007). Such transient conditions made possible the preservation of steep gradients in post-magmatic mineralogy in the chromitite host of these "arteries". Hydrothermal fluids had the potential to crystallize rodingite-related minerals only at the stage they invaded chromitites because of ambient peraluminous conditions prevailing in the chrome ore bodies. Some analogous studies note the potential armor effect of chromitite (e.g., Gosh and Morishita, 2011; Proenza et al., 1999; Zaeimnia et al., 2017), possibly favoring the creation of micro-rodingite veins rather than a pervasive rodingite system.

The Ayios Stefanos chromitites are high-Al, and differ greatly from the geochemical association of their host mantle nappes. The hydrogrossular microveins described in this paper occur exclusively within the chrome ore bodies, not in their hosting lithologies. We consider the establishment of a peraluminous system, petrologically isolated from the ambient lithological environment, in the immediate post-magmatic period as most likely for the formation of micro-rodingites.

5.3. Chemical element mobility as the "feeding" mechanism of microveins

5.3.1. Potential source(s) of Ca

Serpentinization can vigorously destabilize Ca-rich clinopyroxene (diopside) as follows:

$$3CaMgSi_2O_6 + 6H^+_{fluid} \rightarrow Mg_3Si_2O_5(OH)_4 + 3Ca^{2+} + H_2O + 4SiO_{2fluid} \quad (1)$$

If this reaction happens at moderate *T* (>400 °C), the resultant Ca^{2+}-rich fluid would be mildly acidic (Charlou et al., 2002). This fluid may trigger replacement of clinopyroxene by tremolite (Frost and Beard, 2007) as follows:

$$5CaMgSi_2O_6 + 6H^+_{fluid} \rightarrow Ca_2Mg_5Si_8O_{22}(OH)_2 + 3Ca^{2+} + 2H_2O + 2SiO_{2fluid} \quad (2)$$

Tremolite for clinopyroxene substitution is common in the gabbro samples we collected (Fig. 5h). This is coherent with the observation that, in the field, the microveins are spatially related to gabbroic impregnations in the chromitite, and this possibly indicates addition of Ca from outside the system (e.g., Frost et al., 2005).

Plagioclase in gabbro and the plagioclase lherzolite of the hanging wall nappe could arguably serve as a potential source for Ca within the microveins. Chromitites that lack fracture-filling gabbro also lack hydrogrossular-rich microveins, making it hard for plagioclase in lherzolites to serve as a source for Ca within the micro-rodingite veins. If plagioclase in lherzolites would be the source of Ca within the veinlets these would be found in every single ore body of the broader study area due to the armor effect described above. This is not the case for the Ayios Stefanos micro-rodingites. Though we cannot entirely exclude it as a possibility, it is hard to envision that plagioclase in the vein-filling gabbro made significant contributions of Ca to the microveins in the post-magmatic period. Petrographic observations suggest that anorthite in the gabbro intrusions shows only minimal conversion to saussurite along brittle fractures. Furthermore, the replacement of anorthite by saussuritization-derived minerals (i.e., zoisite-

epidote, prehnite) is a Ca-consuming process that has been described by Coleman (1967, 1977) as follows:

$$3CaAl_2Si_2O_8 + Ca^{2+} + 2H_2O \rightarrow 2Ca_2A1_3Si_3O_{12}(OH) + 2H^+ \quad (3)$$

Could Ca be introduced directly from the chromitite hosts to the microveins? Calcium can be removed from Cr-spinel through a lattice distortion mechanism (Mitra, 1973). This, however, would not seem an effective Ca-gaining process with respect to the low CaO (≤0.41 wt%) of Cr-spinel from the Ayios Stefanos chromitites (Kapsiotis et al., 2016).

5.3.2. Potential source(s) of Al, Cr, Fe^{3+} and Ti

Only 1 out of 9 veinlet-hosting chromitite samples demonstrated limited replacement of Cr-spinel by ferrian chromite, excluding the possibility that Al, Cr, Fe^{3+} and Ti were expelled from Cr-spinels during their post-magmatic alteration (e.g., Colás et al., 2014; Gervilla et al., 2012; Mukherjee et al., 2010).

Chromium and Al are known to be only slightly mobile during hydrothermal alteration of ultramafic rocks (e.g., López et al., 1995). Hence, pyroxene and accessory spinel in peridotites seem to be an unrealistic source of Cr and Al within the minerals filling the microveins. Furthermore, these elements, including Ti and Fe^{3+}, do not partition into the olivine lattice (e.g., Pagé and Barnes, 2009). This suggests that the composition of minerals filling the microveins is not greatly influenced by the serpentinization of olivine in peridotites.

The composition of Cr-spinel fragments scattered in the microveins interior is similar to that of the hosting chrome ore boulder (Kapsiotis et al., 2016). Furthermore, some microvein Cr-spinels show evidence for partial dissolution and replacement by Cr-rich hydrogrossular (Fig. 6h). Thus, it is possible that these Cr-spinel relics provided the source of Cr, Al and Fe^{2+} for the low-*T* Cr-bearing minerals (hydrogarnet, chlorite) filling the veinlets. We propose the following reaction to explain Cr-spinel conversion to hydrogrossular:

$$\begin{aligned} &2(Mg,Fe)(Cr,Al)_2O_4 + 3CaO + (4-x)SiO_2 + 2xH_2O + 1.5O_2 \\ &\rightarrow Ca_3(Cr,Al,Fe)_2(SiO_4)_{3-x}(OH)_{4x} + 2MgO_{fluid} + Cr_2O_{3fluid} \\ &\quad + Al_2O_{3fluid} + SiO_{2fluid} \end{aligned} \quad (4)$$

This chemical equation describes a Cr-spinel reaction with an oxidizing aqueous fluid charged with Ca and Si, such as the one produced by Eq. (2). According to this reaction, Fe^{2+} in Cr-spinel will be oxidized to Fe^{3+} in hydrogarnet. The resultant solution would be rich in MgO, SiO_2, Cr_2O_3 and Al_2O_3 that can be combined to form Cr-bearing magnesiosilicates (i.e., clinochlore). We note that neither zoned Cr-spinels nor hydrothermal Cr-spinels such as those observed in mantle and crustal diopsidites from Oman (Akizawa and Arai, 2014; Arai and Akizawa, 2014) were recognized here. This implies that the invading fluid was aggressive enough to drastically dissolve Cr-spinel fragments along their boundaries, as well as that the Cr budget of the resultant fluid preferentially consumed with the precipitation of Cr-rich hydrogrossular and clinochlore.

Chromian spinel dissolution can partly account for the low TiO_2 content in Cr-rich hydrogrossular, but it fails to explain the presence of Ti-rich hydrogrossular in the investigated microveins. It is hard to envision Cr-spinel replacement by Cr-rich hydrogrossular as an effective mechanism for increasing the relative presence of Ti in hydrogarnet. The original content of TiO_2 in Cr-spinels from the chrome ores is low (≤0.21 wt%), and the content of TiO_2 in Cr-spinels from the Ti-rich hydrogrossular-bearing chromitite samples (No. 1 and 3d) is even lower (≤0.15 wt%; Kapsiotis et al., 2016). The fracture-filling gabbro within the chrome ore boulder contains sphenoid titanite as an accessory mineral phase. This titanite could breakdown during the metasomatic alteration of

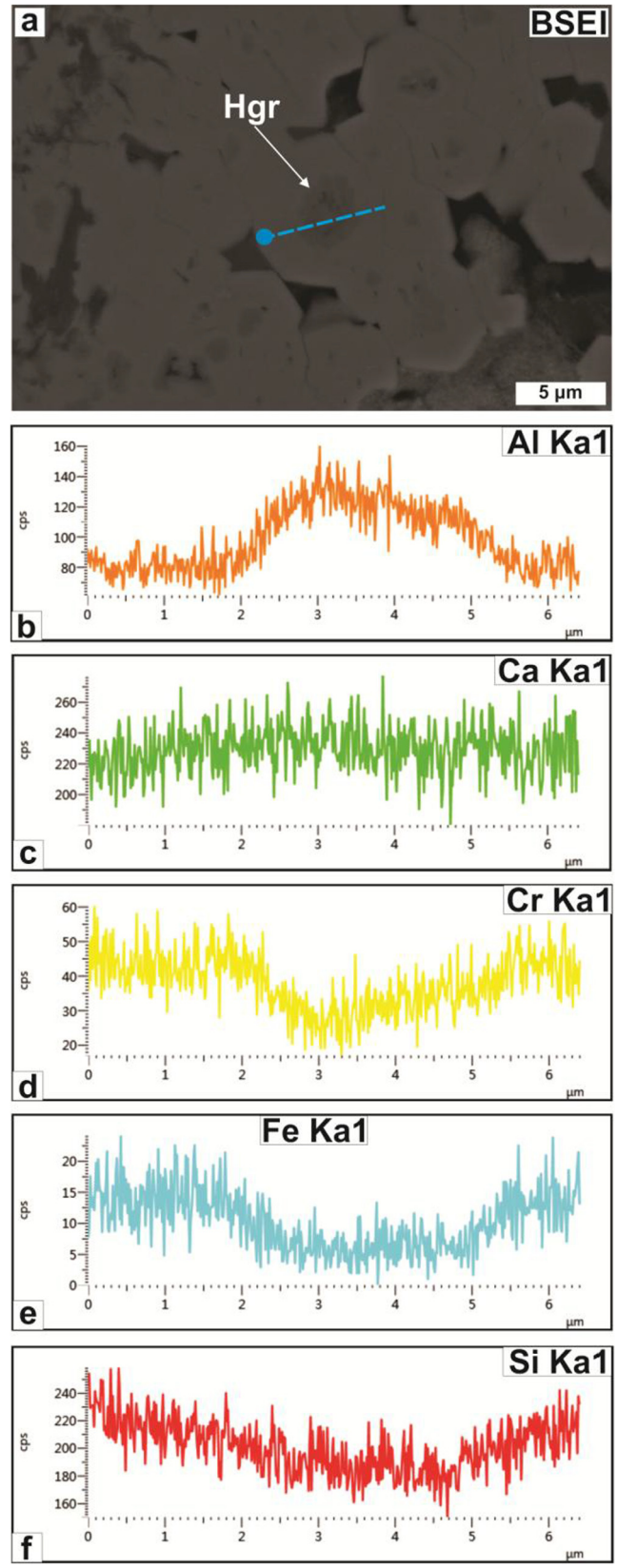

Fig. 10. (a) Back-scattered electron image showing compositionally zoned hydrogrossular grains with voids (dark spots; abbreviations as in previous figures). (b) to (f) Single-element (EDS) core-rim profile line scans of Al, Ca, Cr, Fe and Si demonstrating an evident increase in the hydroandradite and hydrouvarovite content toward the periphery of the analyzed hydrogrossular grain.

the gabbro intrusions as indicated by the porous structure of some titanite grains, facilitating limited release of Ti to the microvein fluid, and thence, the final incorporation of Ti within the crystallizing hydrogarnet lattice.

5.3.3. Chemical element carriers

Grossular has low solubility in pure H_2O at 400–800 °C and up to 10 kb (Fockenberg et al., 2004). However, hydrogrossular/grossular-rich formations of hydrothermal origin are common in various natural settings. Thompson (1975), to explain this conundrum, recommended that the addition of a saline fluid to rocks undergoing metasomatism could substantially enhance their inventory in low solubility components in pure H_2O.

The nature of the element carrier(s) needs to be constrained more precisely by the study of specific characteristics (i.e., fluid inclusions). Nevertheless, the finding of Cr-rich hydrogrossular aggregates surrounded by calcite in some veinlets (Fig. 6g) would suggest hydroxyl- and carbon-bearing ligands. Experimental work (Rai et al., 2007) and geological evidence (Arai and Akizawa, 2014) support that the solubility of Cr may drastically increase in the presence of carbonic alkaline hydrous agents due to its enhanced complexation with carbonates. The presence of sylvite confirms that chlorides must have been another type of complexing ligand contributing to the mobility of Al, Ca and Cr in microveins.

The presence of a CO_3^{2-} - and Cl^--bearing aqueous phase (containing appreciable silicate components that could carry Cr; Akizawa et al., 2016) can be inferred by considering that the whole metasomatic process happened within the constrictional ductile strain regime of an emplacing ophiolitic nappe. Similar deformation conditions have been described within neighboring ophiolitic complexes (i.e., Vourinos; Rassios and Dilek, 2009). The crystallization mechanisms of such sensitive features as the studied microveins must be considered within the co-existing deformation framework of their host geotectonic environment, and indeed, the microveins may aid in the interpretation of some petrological aspects of this environment (see Section 6).

5.4. Qualitative assessment of the physicochemical conditions of microveins formation

Within the ultramafic exposures of the Ayios Stefanos mine, micro-rodingite veins occur within a chromitite body (now preserved as boulder) cut by gabbro; each microvein is an isolated feature, never observed to intersect another veinlet or anastomose. This fabric is a feature imposed from the nature of the initial fractures hosting the vein mineralogy. The en echelon, non-deformed parallel fractures are typical structures of cooling rather than shear processes. Once opened, the fractures remained undeformed and independent, forming disequilibrium microenvironments permitting hydrogrossular precipitation (e.g., Plümper et al., 2014). This disequilibrium is reflected by the nature of the vein-filling material: hydrogrossular spherules are zoned, but do not show oscillatory zoning (Fig. 6e, Fig. 10a); hydrogrossular grades abruptly to chlorite and serpentine within a vein. These textural relations suggest that fracture filling occurred as a result of the establishment of an essentially closed system affected only by minor fluctuations in its thermodynamic parameters.

Thermodynamic parameters can be estimated by the use of combined spectroscopic and chemical data. We document a decrease in H_2O and Al_2O_3 coupled with an increase in SiO_2, Cr_2O_3 and Fe_2O_3 in most hydrogrossular globules from core to rim (Fig. 10; see Table 2 in the supplementary file). This decrease might be related to: (i) narrow thermal stability of hydrogrossular, showing solubility toward an anhydrous end-member stable at higher T, (ii) growth of hydrogrossular spherules in a migrating fluid under decreasing P_{H2O} or (iii) incorporation of H^+ in the structure of neighboring minerals (e.g., Birkett and Trzcienski, 1984). Pressure remained at low levels during the crystallization of hydrogrossular spherules and their adjacent mineralization

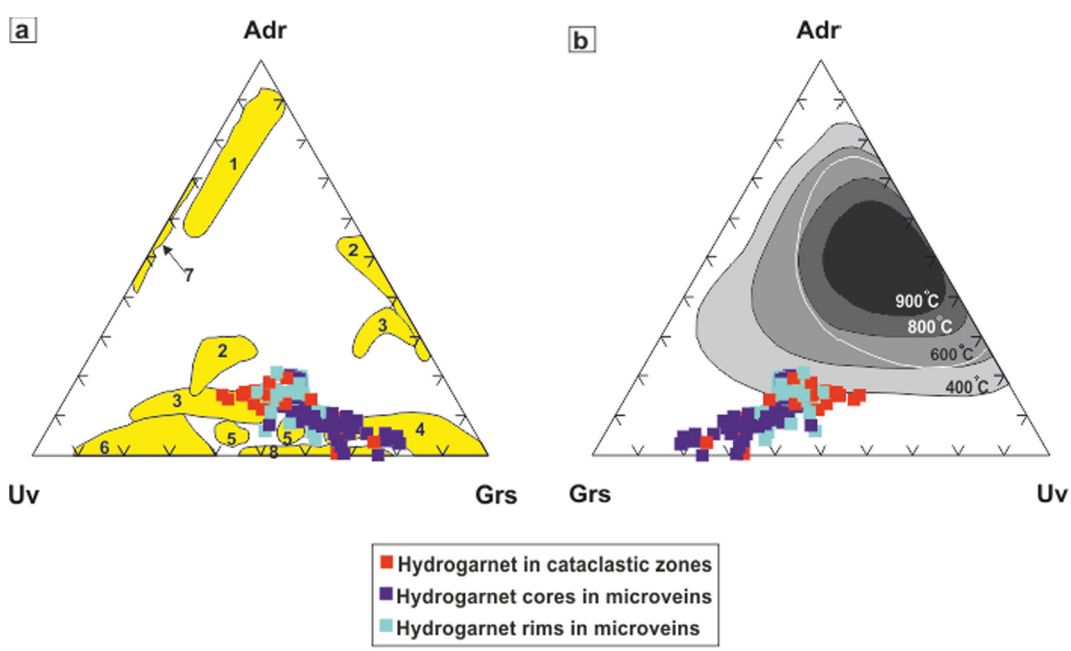

Fig. 11. (a) Compositional plot of the analyzed hydrougrandites (as anhydrous garnets) on the triangular diagram Adr-Grs-Uv and comparison with previously-reported natural Cr-garnet compositions from various areas and geological settings [(1) Reaume Township, Ontario (Duke and Bonardi, 1982); (2) Labrador (Kalamarides and Berg, 1988); (3) White River (Pan and Fleet, 1989); (4) various localities in Canada (Dunn, 1978); (5) Luikonlahti, Finland (von Knorring et al., 1986); (6) Outukumpu, Finland (von Knorring et al., 1986); (7) Sukinda (Orissa), India (Pal and Das, 2010); and (8) Moa-Baracoa massif, Cuba (Proenza et al., 1999)]. (b) Compositional plot of the analyzed hydrougrandites (as anhydrous garnets) on the triangular diagram Adr-Grs-Uv where grey fields are calculated spinodals and the dashed white line represents the approximate position of the solvus at 800 °C (after Ganguly, 1976). Abbreviations: *Adr* andradite, *Grs* grossular, *Uv* uvarovite.

(0.25–3 kb; e.g., O'Hanley et al., 1992). The H_2O content of serpentine and clinochlore cannot be attributed to transfer of OH^- from hydrogrossular, but to a cooler aqueous agent. This dehydration pattern favors a minimal increase in *T* strictly during hydrogarnet crystallization within the microveins.

Temperature considerations are complex. The minerals found within the microveins show a range of crystallization *T*'s, some of which have yet to be adequately established in the literature. The following section describes our documentation of constraints on mineralization from the high end to low end of these *T* requirements:

(i) Stability experiments in the hydrogarnet system: $Ca_3Al_2(SiO_4)_{3-x}(OH)_{4x}$-$Ca_3Cr_2(SiO_4)_{3-x}(OH)_{4x}$-$Ca_3Fe_2(SiO_4)_{3-x}(OH)_{4x}$ have yet to be rigorously investigated. A ternary phase diagram presented by Ganguly (1976), indicates the stability of solid solution in the system andradite-grossular-uvarovite, and calculates spinodals for a range of *T* between 900 and 400 °C; this extends from the uvarovite-andradite join toward the grossular end-member. Using this as analogous to crystallization conditions of microvein hydrougrandites results in the possibility of extensive miscibility along the (hydro)grossular-(hydro)uvarovite join (Fig. 11a) at

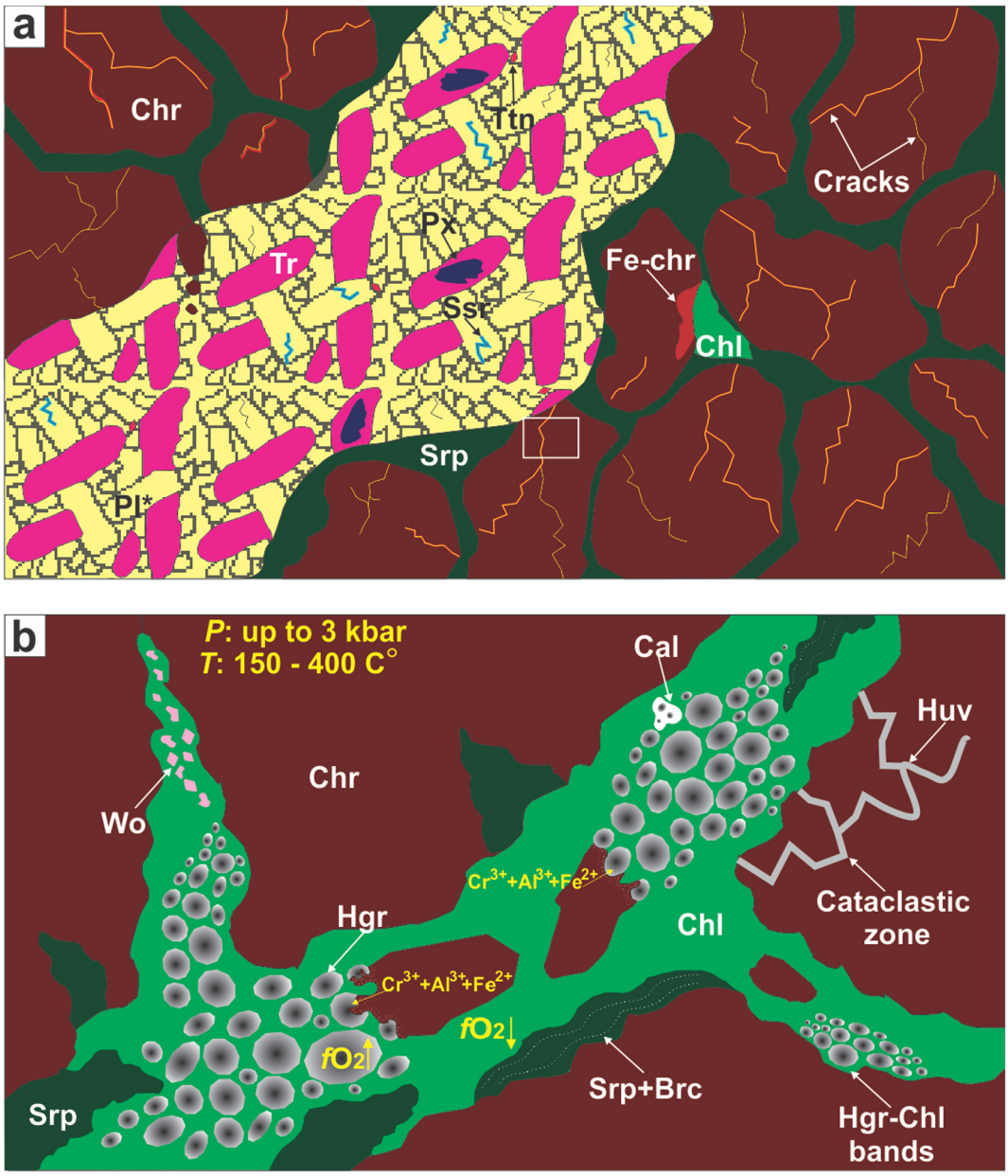

Fig. 12. Graphic model portraying the sequence of igneous and post-magmatic processes recorded in the investigated chromitite boulder from the Ayios Stefanos mantle suite. (a) Intrusion of gabbro in the chromitite at semi-ductile conditions followed by hydrothermal alteration. Cooling of chromitite and opening of brittle cracks that allow oxidizing Ca-rich hydrous fluids resulting from gabbro alteration to move within the ore-making Cr-spinel grains. (b) Close up of a microvein and an adjacent cataclastic zone marked by the white, open square in (a). The Ca-rich fluid will dissolve the boundaries of some Cr-spinel fragments dispersed in the veinlets interior and will be charged with Cr^{3+}, Al^{3+} and Fe^{2+}. Zoned hydrogrossular spherules will precipitate from the fluid, whereas hydrouvarovite will fill the nearby cataclastic zone and hydrougrandite along with or without wollastonite the lateral fringes of some microveins. Variations of the physicochemical conditions during the veinlets formation are also noted. Abbreviations: *Brc* brucite, *Huv* hydrouvarovite, *Pl** plagioclase showing minor alteration to saussurite (*Ssr*), *Ttn* titanite (the rest as in previous figures).

moderate *T's* (400–600 °C; Fig. 11b). We note that these *T's* might be too high, since hydrogrossular has a lower stabilization *T* than that of its anhydrous equivalent (Hsu, 1980). The formation of hydrogrossular-bearing rodingites elsewhere has been attributed to low-*T* (150–350 °C) hydrothermal fluids (e.g., Barriga and Fyfe, 1983; Beard and Hopkinson, 2000). Micro-crystalline observations and the presence of Si-poor minerals (i.e., hydrougrandites, chlorite) in microveins confirm that Si activity was lowered as a response to the development of a serpentinization-related hydrothermal system at *T's* below 400 °C (Bach and Klein, 2009).

(ii) The occurrence of wollastonite in a low-*T* lithology is at odds with the consensus opinion of its formation under conditions of high *T* after devolatilization of calcite- and quartz-rich assemblages. Some studies confirm wollastonite formation at *T's* of 400–450 °C in and around serpentinites (e.g., Malvoisin et al., 2012).

(iii) Vesuvianite forms during advanced rodingitization at *T's* between 300 and 400 °C (e.g., Li et al., 2008).

(iv) Lizardite, the predominant serpentine polymorph in the veinlets, is stable at *T's* up to 300 °C. Lizardite could have formed during the cooling of the enclosed fluids.

(v) Implementation of the geothermometer proposed by Kranidiotis and MacLean (1987) yielded a maximum *T* of 228 °C for clinochlore. That *T* marks the beginning of the closure of the system characterized by a drop in *T*, which is common during vein-filling.

The heat source of the microvein activity can be established by considering several possibilities: (i) intrusion of gabbro within the chromitites could have provided a temporary rise in local *T* conditions; however, such intrusion could not be considered as a sustainable thermal source maintaining advective heat. (ii) Tribological processes within the deforming zone could be a heat source, but can be discounted for the following reasons: experimental studies show that serpentine has a low (internal) friction coefficient (Iyer et al., 2008) and the presence of brucite within the serpentine-dominant lithologies reduces their strength properties even more (Moore et al., 2001). These would limit conversion of mechanical work into heat in microveins, but more important, the microvein materials, even though structurally highly incompetent, are not deformed. (iii) Fyfe and Lonsdale (1981) and Iyer et. al. (2008) consider that heat release could be explained as concurrent to serpentinization. Volume expansion during serpentinization of the surrounding peridotites could account for the formation of fractures, but such fractures are not observed in these rocks. However, some Cr-spinels within Ayios Stefanos ultramafics demonstrate rather typical pull apart structures attributed to serpentinization. Such structures are not apparent in chromitites. More precise investigation into the brittle phase response of the spinel structure is required to understand this issue.

We do not believe that it is not necessary to invent a local source of heat for the hydrothermal fluids responsible for the microveins. The *T* estimates deduced from mineralogy, with an uppermost limit of ~400 °C required, and cessation of mineralization at ~150 °C, are in agreement with the ambient *T* present within a cooling oceanic lithospheric slab (e.g., Rassios and Dilek, 2009).

The composition of the hydrothermal fluids responsible for the formation of microveins can also be approximated by their mineralogy as follows:

(i) The presence of hydrogrossular with dissolved hydroandradite in the veinlets necessitates precipitation from a rich-in-Ca, Fe^{3+}-bearing fluid (Barriga and Fyfe, 1983) such as the one resulting from alteration of gabbro (Fig. 12a). A minor increase in the hydroandradite molecule from core to rim could be due to slightly higher fO_2 conditions during the final stages of hydrogrossular nucleation. Oxidation of Fe^{2+} during the formation of hydroandradite would maintain a low fO_2 level following hydrogrossular spherules precipitation (Fig. 12b), and this would permit millerite desulfurization.

(ii) Low *T* wollastonite has been suggested as a possible marker of reducing conditions (Fig. 12b) in agreement with the reducing environment present during serpentinization (Malvoisin et al., 2012).

(iii) Brucite with lizardite in the veinlets constrain silica activity to extremely low levels (i.e., at 200 °C $log aSiO_2,aq \leq -6$; Plümper et al., 2014).

(iv) The presence of calcite indicates alkaline conditions [$pH = -\log(aH^+) > 7$] during the initial stages of the microvein-filling process.

From these relations, it would appear that precipitation of hydrogrossular causes a decrease in the chemical potential μ (CaO/MgO) ratio of the system favouring late-stage crystallization of magnesiosilicates.

6. Conclusions

Microveins are very small features, but our study of the hydrous activity responsible for their mineral genesis has large implications for the evolution of lithospheric slabs created in ridgecrest spreading.

The knowledge-base of the deformational history of the broader Ayios Stefanos mine area is well established (Rassios and Dilek, 2009; Rassios and Konstantopoulou, 1993). Peridotite exposures within the retired chrome mine document post-ridgecrest ductile deformation concurrent to the initiation of nappe formation. Late ridgecrest-related gabbroic magma intruded a ductile-brittle thrust provided by a mechanically sheared dunite entrapped between the nappes; this dunite is host to cataclastic-textured (mechanically deformed synchronous to ductile deformation) chrome ore bodies. Deformation of peridotite provides a rough scale for estimating *P-T* in the slab (Rassios and Smith, 2000), but only to the termination of ductile deformation conditions (Grieco and Merlini, 2012; Python et al., 2007). In the post-ductile phase of the cooling lithospheric slab, almost nothing is known of evolving slab conditions. There is no evidence within these rocks of post-ophiolitic metamorphism or *syn*-ophiolitic fluctuating *T* in this period. What we see are just cooling conditions within an oceanic plate in drift conditions.

The Ayios Stefanos microveins occur in en echelon fractures characteristic of cooling processes. However, what *T's* are present in massive chromitites during this cooling phase are also unknown; seemingly brittle features can form in Cr-spinel at *T's* consistent with ductile conditions in neighboring minerals. We have also documented textural evidence that Cr-spinel marginal to these veins could have undergone limited annealing/recrystallization, processes aided by hot fluid activity. This implies the existence of a curious phase of deformation-mineralization that can only be resolved by microveins investigation.

The Ayios Stefanos microveins are filled with hydrogrossular spherules, clinochlore and serpentine, an assemblage which is reminiscent of rodingites. This mineralogy was caused *via* microvein-filling by small quantities of a Ca-rich hydrothermal fluid; the source of Ca in a mantle section such as that present at Ayios Stefanos could be found within plagioclase lherzolite, within influxes of fluids from (unexposed) neighboring mafic cumulate

rocks, or from the intruding gabbro. In the case of the chromitite-hosted microveins, formed proximal to ore-intruding gabbro, we think that liquids accompanying tremolitization of clinopyroxene in the gabbroic veins, with concurrent addition of Al, Cr and Fe^{2+} liberated from the partial dissolution of Cr-spinel fragments, provide the most likely source of mineralization fluids.

The *T* of formation of the microveins ranges between 400 °C to no lower than 150 °C, suggesting a local provenance and mechanism for their hydrothermal activity. These are observations of the environment present within a rift-produced lithosphere during a late period of cooling. Therefore, the studied microveins offer an opportunity for understanding the conditions preceding final emplacement and cessation of high-*T* phenomena within obducted ophiolites.

Conflicts of interest

We declare no conflict of interest. The funding sponsors had no role in the design of the study, in the collection, analyses or interpretation of data, in the writing of the manuscript, and in the decision to publish the results.

Acknowledgements

Franco Pirajno, Editor-in-Chief of Ore Geology Reviews, and Sisir K. Mondal, Guest Editor of the Special Issue "Chromite: Petrogenetic Indicator to Ore Deposits", are thanked for the editorial handling of this paper. We are grateful to Drs. T. Morishita, K. Sajeev and S. Arai for their constructive feedback and helpful comments, which greatly improved some earlier versions of our manuscript. Research was partly supported by Sun Yat-sen University Special Fund Project (Young Faculty's Research Start-up Grant No. 32110-31121401) and the National Natural Science Foundation of China (NNSFC; Youth Science Fund Project No. 41402065).

Appendix A. Supplementary data

Supplementary data associated with this article can be found, in the online version, at http://dx.doi.org/10.1016/j.oregeorev.2017.06.006.

References

Akizawa, N., Arai, S., 2014. Petrology of mantle diopsidite from Wadi Fizh, northern Oman ophiolite: Cr and REE mobility by hydrothermal solution. Isl. Arc. 23, 312–323.
Akizawa, N., Tamura, A., Fukushi, K., Yamamoto, J., Mizukami, T., Python, M., Arai, S., 2016. High-temperature hydrothermal activities around suboceanic Moho: an example from diopsidite and anorthosite in Wadi Fizh, Oman ophiolite. Lithos 263, 66–87.
Andrut, M., Wildner, M., 2001. The crystal chemistry of birefringent natural uvarovites: Part I. Optical investigations and UV-VIS-IR absorption spectroscopy. Am. Mineral. 86, 1219–1230.
Arai, S., 1994. Characterization of spinel peridotites by olivine-spinel compositional relationships: review and interpretation. Chem. Geol. 113, 191–204.
Arai, S., Akizawa, N., 2014. Precipitation and dissolution of chromite by hydrothermal solutions in the Oman ophiolite: new behavior of Cr and chromite. Am. Mineral. 99 (1), 28–34.
Arai, S., Okamura, H., Kadoshima, K., Tanaka, C., Suzuki, K., Ishimaru, S., 2011. Chemical characteristics of chromian spinel in plutonic rocks: implications for deep magma processes and discrimination of tectonic setting. Island Arc 20, 125–137.
Arredondo, E.H., Rossman, G.R., 2002. Feasibility of determining the quantitative OH content of garnets with Raman spectroscopy. Am. Mineral. 87, 307–312.
Austrheim, H., Prestvik, T., 2008. Rodingitization and hydration of the oceanic lithosphere as developed in the Leka ophiolite, north-central Norway. Lithos 104, 177–198.
Bach, W., Klein, F., 2009. The petrology of seafloor rodingites: insights from geochemical reaction path modeling. Lithos 112, 103–117.
Bailey, S.W., 1980. Summary of recommendations of AIPEA nomenclature committee on clay minerals. Am. Mineral. 65, 1–7.
Barnes, S.J., 2000. Chromite in komatiites, II. Modification during greenschist to mid-amphibolite facies metamorphism. J. Petrol. 41, 387–409.
Barriga, F., Fyfe, W.S., 1983. Development of rodingite in basaltic rocks in serpentinites, East Liguria. Italy. *Contrib. Min. Petrol.* 84, 146–151.
Barth, M.G., Mason, P.R.D., Davies, G.R., Drury, M.R., 2008. The Othris Ophiolite, Greece: a snapshot of subduction initiation at a mid-ocean ridge. Lithos 100, 234–254.
Beard, J.S., Hopkinson, L., 2000. A fossil, serpentinization-related hydrothermal vent, Ocean Drilling Program Leg 173, Site 1068 (Iberia Abyssal Plain): some aspects of mineral and fluid chemistry. J. Geophys. Res. 105, 16527–16539.
Birkett, T.C., Trzcienski Jr., W.E., 1984. Hydrogarnet: multi-site hydrogen occupancy in the garnet structure. Can. Min. 22, 675–680.
Challis, A., Grapes, R., Palmer, K., 1995. Chromian muscovite, uvarovite, and zincian chromite: products of regional metasomatism in northwest Nelson, New Zealand. Can. Min. 33, 1263–1284.
Charlou, J.L., Donval, J.P., Fouquet, Y., Jean-Baptiste, P., Holm, N., 2002. Geochemistry of high H_2 and CH_4 vent fluids issuing from ultramafic rocks at the Rainbow hydrothermal field, (36°14′N, MAR). Chem. Geol. 191, 345–359.
Colás, V., González-Jimenéz, J.M., Griffin, W.L., Fanlo, I., Gervilla, F., O'Reilly, S.Y., Pearson, N.J., Kerestedjian, T., Proenza, J.A., 2014. Fingerprints of metamorphism in chromite: new insights from minor and trace elements. Chem. Geol. 389, 137–152.
Coleman, R.G., 1967. Low-temperature reaction zones and alpine ultramafic rocks of California, Oregon and Washington. *U.S.* Geol. Surv. Bull. 1247, 1–49.
Coleman, R.G., 1977. Ophiolites. Ancient Oceanic Lithosphere? Springer, Berlin-Heidelberg-New York, pp. 1–229.
Duke, J.M., Bonardi, M., 1982. Chromian andradite from Reaume Township. Ontario. *Can. Mineral.* 20, 49–53.
Dunn, P.J., 1978. On the composition of some Canadian green garnets. Can. Mineral. 16, 205–206.
Dick, H.J.B., Bullen, T., 1984. Chromian spinel as a petrogenetic indicator in abyssal and alpine-type peridotites and spatially associated lavas. Contrib. Min. Petrol. 86, 54–76.
Dunn, P.J., Fleischer, M., Langley, R.H., Shigley, J.E., Zilczer, J.A., 1985. New mineral names. Am. Mineral. 70, 871–881.
Ferrière, J., Bertrand, J., Simantov, J., De Wever, P., 1988. Comparison entre les formations volcano–detritiques (Mélanges) du malm des Hellenides internes (Othrys, Eubee): implications geodynamics. B. Geol. Soc. Greece 20, 223–235.
Fockenberg, T., Burchard, M., Maresch, W.V., 2004. Solubilities of calcium silicates at high pressures and temperatures. Lithos 73, S37.
Frost, B.R., 1975. Contact metamorphism of serpentinite, chloritic blackwall and rodingite at Paddy-Go-Easy Pass, Central Cascades, Washington. J. Petrol. 16, 272–313.
Frost, B.R., Beard, J.S., 2007. On silica activity and serpentinization. J. Petrol. 48, 1351–1368.
Frost B.R., Beard J.S., Abratis M.W., Andreani M., Delacour A., Drouin M., Fryer P., McCaig A., Nozaka T., Ohara Y. and the shipboard scientific parties of IODP expeditions 304 and 305, 2005. Importance of silica activity to the serpentinization processes: insights from micro-rodingites in IODP hole U1309D. EOS, Trans. Am. Geophys. Union, Abstract V51B–1483.
Fyfe, W.S., Lonsdale, P., 1981. Ocean floor hydrothermal activity. In: Emiliani, C. (Ed.), The Sea, vol. 7. Wiley and Sons, New York, pp. 589–638.
Ganguly, J., 1976. The energetics of natural garnet solid solution. II. Mixing of the calcium silicate end-members. Contrib. Mineral. Petr. 55, 81–90.
Gervilla, F., Padron-Navarta, J.A., Kerestedjian, T., Sergeeva, I., González-Jiménez, J. M., Fanlo, I., 2012. Formation of ferrian chromite in podiform chromitites from the Golyamo Kamenyane serpentinite, Eastern Rhodopes, SE Bulgaria: a two stage process. Contrib. Mineral. Petr. 164, 643–657.
Gosh, B., Morishita, T., 2011. Andradite-uvarovite solid solution from hydrothermally altered podiform chromitite, Rutland ophiolite, Andaman India. Can. Mineral. 49, 573–580.
Grew, E.S., Locock, A.J., Mills, S.J., Galuskina, I.O., Galuskin, E.V., Hålenius, U., 2013. Nomenclature of the garnet supergroup. Am. Mineral. 98, 785–811.
Grieco, G., Merlini, A., 2012. Chromite alteration processes within Vourinos ophiolite. Int. J. Earth Sci. 101 (6), 1–11.
Heflik, W., Żabiński, W., 1969. A chromian hydrogrossular from Jordanów, Lower Silesia. Poland. *Mineral. Mag.* 37, 241–243.
Hsu, L.C., 1980. Hydration and phase relations of grossular-spessartine garnets at PH_2O = 2 kb. Contrib. Mineral. Petr. 71, 407–425.
Iyer, K., Jamtveit, B., Mathiesen, J., Malth-Sørenssen, A., Feder, J., 2008. Reaction-assisted hierarchical fracturing during serpentinization. Earth Planet. Sci. Lett. 267, 503–516.
James, B.R., 2003. Chromium. In: Stewart, B.A., Howell, T.A. (Eds.), Encyclopedia of Water Science. Marcel Dekker Inc., pp. 77–82.
Kalamarides, R.I., Berg, J.H., 1988. Coexisting Cr-rich and Cr-poor garnet from a calc-silicate gneiss. Labrador. *Can. Mineral.* 26, 335–342.
Kapsiotis, A., Ewing, Rassios A., Antonelou, A., Tzamos, E., 2016. Genesis and multi-episodic Alteration of zircon-bearing chromitites from Ayios Stefanos, Othris Massif, Greece: assessment of an unconventional hypothesis on the origin of zircon in ophiolitic chromitites. Minerals 6 (4), 124. http://dx.doi.org/10.3390/min6040124.
Kitamura, K., Iyi, N., Kimura, S., Chevrier, F., Devignes, J.M., Le Gall, H., 1986. Growth-induced optical anisotropy of epitaxial garnet films grown on (110)-oriented substrates. J. Appl. Phys. 60, 1486–1489.
Kolesov, B.A., Geiger, C.A., 1998. Raman spectra of silicate garnets. Phys. Chem. Miner. 25, 142–151.

Kolesov, B.A., Geiger, C.A., 2005. The vibrational spectrum of synthetic hydrogrossular (katoite) $Ca_3Al_2(O_4H_4)_3$: a low-temperature IR and Raman spectroscopic study. Am. Mineral. 90, 1335–1341.
Koutsovitis, P., Magganas, A., Pomonis, P., Ntaflos, T., 2013. Subduction-related rodingites from East Othris, Greece: mineral reactions and physicochemical conditions of formation. Lithos 172–173, 139–157.
Kranidiotis, P., MacLean, W.H., 1987. Systematics of chlorite alteration at the Phelps Dodge massive sulphide deposit, Matagami. Quebec. *Econ. Geol.* 82, 1898–1911.
Lager, G.A., Armbruster, T., Rotella, F.J., Rossman, G.R., 1989. OH substitution in garnets: X-ray and neutron diffraction, infrared, and geometric-modeling studies. Am. Mineral. 74, 840–851.
Leblanc, M., Nicolas, A., 1992. Ophiolitic chromites. Int. Geol. Rev. 34, 653–686.
Li, X.P., Zhang, L., Wei, C., Ai, Y., Chen, J., 2007. Petrology of rodingite derived from eclogite in western Tianshan. China. *J. Metamorph. Geol.* 25, 363–382.
Li, X.P., Rahn, M., Bucher, K., 2008. Eclogite facies metarodingites - phase relations in the system SiO2–Al2O3–Fe2O3–FeO–MgO–CaO–CO2–H2O: an example from the Zermatt-Saas ophiolite. J. Metamorph. Geol. 26, 347–364.
Locock, A.J., 2008. An excel spreadsheet to recast analyses of garnet into end-member components, and a synopsis of the crystal chemistry of natural silicate garnets. Comput. Geosci. 34, 1769–1780.
López, Sánchez.-Vizcaíno V., Franz, G., Gómez-Pugnaire, M.T., 1995. The behavior of Cr during metamorphism of carbonate rocks from the Nevado-Filabride Complex, Betic Cordilleras. Spain. *Can. Mineral.* 33, 85–104.
Malvoisin, B., Chopin, C., Brunet, F., Galvez, M.E., 2012. Low-temperature wollastonite formed by carbonate reduction: a marker of serpentinite redox conditions. J. Petrol. 53, 159–176.
Melcher, F., Grum, W., Simon, G., Thalhammer, T.V., Stumpfl, E.F., 1997. Petrogenesis of the ophiolitic giant chromite deposits of Kempirsai, Kazakhstan: a study of solid and fluid inclusions in chromite. J. Petrol. 38 (10), 1419–1458.
Meyer, H.O.A., Boyd, F.R., 1972. Composition and origin of crystalline inclusions in natural diamonds. Geochim. Cosmochim. Acta 36, 1255–1273.
Mitra, S., 1973. Mineralogy and paragenesis of Cr-chlorites and uvarovites in chromites of Sukinda, Orissa. India. *Neues Jb. Miner. Monat.* H3, 139–148.
Miura, M., Arai, S., 2014. Platinum-group element and mineral characteristics of sub-arc chromitite xenoliths from the Takashima alkali basalt, southwest Japan Arc. Can. Mineral. 52, 899–916.
Mondal, S.K., Zhou, M.-F., 2010. Enrichment of PGE through interaction of evolved boninitic magmas with early formed cumulates in a gabbro–breccia zone of the Mesoarchean Nuasahi massif (eastern India). Mineral. Depos. 45, 69–91.
Mondal, S.K., Baidya, T.K., Rao, K.N.G., Glascock, M.D., 2001. PGE and Ag mineralization in a breccia zone of the Precambrian Nuasahi ultramafic-mafic complex, Orissa India. Can. Mineral. 39, 979–996.
Moore, D.E., Lockner, D.A., Iwata, K., Tanaka, A., Byerlee, J.D., 2001. How brucite may affect the frictional properties of serpentinite. U. S. Geol. Surv. Open-File Rep., 1–320
Morán-Miguélez, E., Alario-Franco, M.A., Joubert, J.C., 1986. Hydrothermal synthesis and field of existence of silicon-free garnets. Mater. Res. Bull. 21, 107–113.
Mukherjee, R., Mondal, S.K., Rosing, M.T., Frei, R., 2010. Compositional variations in the Mesoarchean chromites of the Nuggihalli schist belt, Western Dharwar Craton (India): potential parental melts and implications for tectonic setting. Contrib. Mineral. Petr. 160, 865–885.
O'Hanley, D.S., Schandl, E.S., Wicks, F.J., 1992. The origin of rodingites from Cassiar, British Columbia, and their use to estimate T and $P(H_2O)$ during serpentinization. Geochim. Cosmochim. Acta 56, 97–108.
Pagé, P., Barnes, S.-J., 2009. Using trace-elements in chromites to constrain the origin of podiform chromitites in the Thetford Mines Ophiolite, Québec, Canada. Econ. Geol. 104, 997–1018.
Pal, T., Das, D., 2010. Uvarovite from chromite-bearing ultramafic intrusives, Orissa, India, a crystal-chemical characterization using ^{57}Fe Mossbauer spectroscopy. Am. Mineral. 95 (6), 839–843.
Pan, Y., Fleet, M.E., 1989. Cr-rich calc-silicates from the Hemlo area. Ontario. *Can. Mineral.* 27, 565–577.
Passaglia, E., Rinaldi, R., 1984. Katoite, a new member of the $Ca_3Al_2(SiO_4)_3$-$Ca_3Al_2(OH)_{12}$ series and a new nomenclature for the hydrogrossular group of minerals. B. Mineral. 107, 605–618.
Plümper, O., Beinlich, A., Bach, W., Janots, E., Austrheim, H., 2014. Garnets within geode-like serpentinite veins: Implications for element transport, hydrogen production and life-supporting environment formation. Geochim. Cosmochim. Acta 141, 454–471.
Proenza, J., Solé, J., Melgarejo, J.C., 1999. Uvarovite in podiform chromitite: the Moa-Baracoa ophiolitic massif. Cuba. *Can. Mineral.* 37, 679–690.
Python, M., Ceuleneer, G., Ishida, Y., Barrat, J.-A., Arai, S., 2007. Oman diopsidites: a new lithology diagnostic of very high temperature hydrothermal circulation in mantle peridotite below oceanic spreading centres. Earth Planet. Sci. Lett. 255, 289–305.
Rai, D., Moore, D.A., Jess, N.J., Rosso, K.M., Rao, L., Heald, S.M., 2007. Chromium (III) hydroxide solubility in the aqueous K^+-H^+-CO_2-HCO_3^{2-}-H_2O system: a thermodynamic model. J. Solution Chem. 36, 1261–1285.
Rassios, A., 1981. Geology and Evolution of the Magmatic Rocks of the Vourinos Ophiolite, Northern Greece (Unpublished Ph.D. thesis). University of California, Davis, USA, pp. 1–594.
Rassios, A., 2013. Cooperative Development for Greek Chromite Reserves. Institute of Geology and Mineral Exploration Report, Greece Regional Office of West Macedonia, pp. 1–28.
Rassios, A., Dilek, Y., 2009. Rotational deformation in the Jurassic Mesohellenic Ophiolites, Greece, and its tectonic significance. Lithos 108, 207–223.
Rassios, A., Konstantopoulou, G., 1993. Emplacement tectonism and the position of chrome ores in the Mega Isoma peridotites, SW Othris. Greece. *B. Geol. Soc. Greece* 28, 463–474.
Rassios, A., Smith, A., 2000. Constraints on the formation and emplacement age of western Greek ophiolites (Vourinos, Pindos and Othris) inferred from deformation structures in peridotites. In: Dilek, Y., Moores, E.M., Elthon, D., Nicolas, A. (Eds.), Ophiolites and Oceanic Crust: New Insights From Field Studies and Ocean Drilling Program, vol. 349, pp. 473–483 (Geol. S. Am. S.).
Smith, A., 1979. Othris, Pindos and Vourinos ophiolites and the Pelagonian zone. In: 6th Colloquium on the Geology of the Aegean Region. Institute of Geological and Mining Research, Athens, Greece, pp. 1369–1374.
Smith, A.G., Hynes, A.J., Menzies, M., Nisbet, E.G., Price, I., Welland, M.J., Ferrière, J., 1975. The stratigraphy of the Othris Mountains, eastern central Greece: a deformed Mesozoic continental margin sequence. Eclogae Geol. Helv. 68, 463–481.
Spray, J.G., Bébien, J., Rex, D.C., Roddick, J.C., 1984. Age constraints on the igneous and metamorphic evolution of the Hellenic-Dinaric ophiolites. In: Dixon, J.E., Robertson, A.H.F. (Eds.), The Geological Evolution of the Eastern Mediterranean, vol. 17. Geol. Soc. Lon. S. Publ., pp. 619–627.
Thomas, S.M., Thomas, R., Davidson, P., Reichart, P., Koch-Müller, M., Dollinger, G., 2008. Application of Raman spectroscopy to quantify trace water concentrations in glasses and garnets. Am. Mineral. 93, 1550–1557.
Thompson, A.B., 1975. Calc-silicate diffusion zones between marble and pelitic schist. J. Petrol. 16, 314–346.
Vergely, P., 1976. Origine «vardarienne», chevauchement vers l'Ouest et rétrocharriage vers l'Est des ophiolites de Macédoine (Grèce) au cours du Jurassique supérieur-Eocrétacé. C. *R. Acad. Sci. Paris* 280, 1063–1066.
von Knorring, O., Condliffe, E., Tong, Y.L., 1986. Some mineralogical and geochemical aspects of chromium-bearing skarn minerals from northern Karelia. Finland. *Bull. Geol. Soc. Finland* 58, 277–292.
Whitney, D.L., Evans, B.W., 2010. Abbreviations for names of rock-forming minerals. Am. Mineral. 95, 185–187.
Zabiński, W., 1966. Hydrogarnets. Polska Akademia Nauk, Oddzial Krakowie, Komisja Nauk Mineralogicznych, Prace Mineralogiczne, vol. 3, pp. 1–69.
Zaeimnia, F., Arai, S., Mirmohammadi, M., 2017. Na-rich character of metasomatic/metamorphic fluids inferred from preiswerkite in chromitite pods of the Khoy ophiolite in Iran: role of chromitites as capsules of trapped fluids. Lithos 268–271, 351–363.